# Elucidating the obligate nature and biological capacity of an invasive fungal corn pathogen

Joshua S. MacCready‡, Emily M. Roggenkamp‡, Kristi Gdanetz and Martin I. Chilvers*

Department of Plant, Soil and Microbial Sciences, Michigan State University, East Lansing, MI 48824, USA.

*Corresponding author: chilvers@msu.edu

‡ Authors have contributed equally to this work

## Abstract

Tar spot is a devasting corn disease caused by the obligate fungal pathogen *Phyllachora maydis*. Since its initial identification in the United States in 2015, *P. maydis* has become an increasing threat to corn production. Despite this, *P. maydis* has remained largely understudied at the molecular level due to difficulties surrounding its obligate lifestyle. Here, we generated a significantly improved *P. maydis* nuclear and mitochondrial genome using a combination of long- and short-read technologies and also provide the first transcriptomic analysis of primary tar spot lesions. Our results show that *P. maydis* is deficient in inorganic nitrogen utilization, is likely heterothallic, and encodes for significantly more protein coding genes, including secreted enzymes and effectors, than previous determined. Furthermore, our expression analysis suggests that following primary tar spot lesion formation, *P. maydis* might reroute carbon flux away from DNA replication and cell division pathways and towards pathways previously implicated in having significant roles in pathogenicity, such as autophagy and secretion. Together, our results identified several highly expressed unique secreted factors that likely contribute to host recognition and subsequent infection, greatly increasing our knowledge of the biological capacity of *P. maydis*, which have much broader implications for mitigating tar spot of corn.

## Introduction

Tar spot is a devastating foliar disease of corn caused by the obligate fungal pathogen *Phyllachora maydis* (Sordariomycete; Phyllachorales; Phyllachoraceae). Tar spot initially appears as a small yellow-brown lesion that quickly transitions into raised irregular-shaped black lesions following melanization **(Figure 1A) (Hock et al., 1995)**. Originally a disease identified in 1904 and endemic to Central and South America, tar spot was first reported in the United States in 2015 **(Maublanc, 1904; Ruhl et al., 2015; da Silva et al., 2021)**. Since 2015, tar spot has rapidly spread further each year and is now present in 15 states and Ontario, Canada where it has caused significant yield loss; tar spot caused an estimated ~ $1.2B in yield loss in 2021 alone **(Figure 1B) (Ruhl et al., 2015; Mueller et al., 2020; Mueller et al., 2022)**.

Despite its significant threat to agriculture, little information is currently known about the molecular mechanisms that contribute to the *P. maydis* disease cycle (i.e., host recognition, plant tissue infiltration, disease progression, reproduction, and subsequent spore dispersal) due to its obligate nature **(Valle-Torres et al., 2020)**. Indeed, all attempts of culturing *P. maydis* have failed and inoculations have remained inconsistent **(da Silva et al., 2021)**, limiting our ability to study the molecular mechanisms of this pathogen. Furthermore, the *P. maydis* disease cycle reports a 12 to 20 day latent period, and early infection has not been extensively studied **(Breunig et al. 2023)**. Given these limitations, other studies have demonstrated that genomic and transcriptomic analyses are powerful tools for studying agriculturally-important obligate ascomycetes, such as *Blumeria graminis* of barley, as well as obligate basidiomycetes, such as *Puccinia graminis* of wheat and barley, *Ustilago maydis* of corn, and *Tilletia indica* of wheat, and provided a crucial foundation upon which further molecular work was made feasible **(Both et al., 2005; Skibbe et al., 2010; Singh et al., 2020; Henningsen et al., 2021)**.

Genomic and transcriptomic studies of obligate fungal plant pathogens have illuminated several cellular and metabolic processes and pathways highly expressed during disease emergence and progression, including: (i) nutrient transporters **(Lanver et al., 2018)**, (ii) glycolysis, lipid degradation, and glycogen utilization **(Both et al., 2005)**, (iii) secretion of effectors and cell wall degrading enzymes **(Presti et al., 2015; Mapuranga et al., 2022)**, (iv) mitogen-activated protein kinases (MAPK) signaling **(Guo et al., 2011)**, and (v) autophagy **(Liu et al., 2016)**. Likewise, many obligate fungi utilize environmental cues, such as light quality and intensity, to modulate essential cellular processes such as asexual and sexual reproduction, spore germination, vegetative growth, nutrient uptake, secondary metabolism, and pathogenicity **(Yu and Fischer, 2019)**. In addition to cellular and metabolic changes during primary infection, all obligate fungi also secrete enzymes, such as those that degrade plant cell walls, as well as effectors, small cysteine-rich virulence factors, to infiltrate host cells and suppress immune responses **(Stergiopoulos and Wit, 2009)**. Whether the genome of *P. maydis* exhibits degradation in primary or secondary metabolic pathways or encodes for canonical light-sensing proteins is currently unknown. Likewise, the cellular and metabolic pathways, as well as the secreted enzymes and effectors, that are highly expressed during primary tar spot lesion formation remain outstanding questions.

Recently, a draft genome assembly of *P. maydis* was announced **(Telenko et al., 2020)**. However, this assembly was largely incomplete (11,228 scaffolds) and annotations lacked transcript evidence. Here, we report a significantly improved *P. maydis* genome assembly consisting of 12 nuclear fragments (1 scaffold and 11 contigs) and the complete circular mitochondrial genome. Comparative genomic analysis identified that *P. maydis* has significant degradation within inorganic nitrogen utilization pathways, potentially accounting for the obligate lifestyle of *P. maydis*, and is a phenomenon also observed in obligate rust fungi. Furthermore, tar spot transcriptomic analysis suggests that following conidia and ascospore formation, carbon flux from respiration and glycolysis is primarily routed away from DNA replication and cell division and towards autophagy and protein export during primary tar spot lesion formation. Importantly, we identified that 6 out of the top 27 highest expressed genes in our analysis were predicted effectors unique to *P. maydis*, a result that illuminates the importance of these secreted factors in tar spot disease. Together, these results provide significant insight into the obligate lifestyle of *P. maydis*, identify cellular and metabolic pathways that are significantly expressed in

primary tar spot lesions, elucidate secreted enzymes and effectors important for tar spot disease, and have much broader implications for mitigating tar spot disease of corn.

## Results and Discussion

### A Near-Chromosomal Genome Assembly

The ability to better understand the precise biological capacity of plant pathogens requires a complete high-quality annotated genome. While great efforts were recently made to generate the first draft genome assembly of *Phyllachora maydis*, termed PM01, this assembly remained largely incomplete partly due to the discovery of high levels of unclassified repetitive regions throughout the genome that complicated assembly with Illumina short reads **(Telenko, et al., 2020)**. Therefore, to account for this issue, we first isolated high molecular weight DNA from an enrichment of conidia mechanically removed from lesions on corn leaf surfaces. We then generated a draft assembly, designated PM02, using long reads generated from two independent Oxford Nanopore PromethION runs, followed by error correction using Illumina short reads. Given the known difficulty in computationally predicting fungal introns and exons, we utilized an RNA-informed approach using HISAT2 and BRAKER2 to accurately annotate PM02 **(Kim et al., 2015, Brůna et al., 2021)**. This approach enabled us to simultaneously annotate our genome and analyze gene expression at primary tar spot lesion formation.

Our approach yielded a high-quality haploid nuclear genome ~64 Mbp in size distributed over 12 fragments (1 scaffold and 11 contigs), as well as the complete ~66 kbp circular mitochondrial genome **(Figure 1C)**. K-mer-based analysis predicted a genome size that was within 2.5 % of our PM02 assembly **(Supplementary Figure 1A)** and BUSCO predicted that PM02 was 98.6% complete, likely the maximum obtainable measure due to the obligate lifestyle of *P. maydis* **(Vurture et al., 2017; Manni et al., 2021)**. Consistent with the previous findings for PM01 (~56 % repetitive content), we found that PM02 contained ~59 % repetitive content, of which, ~54 % was classified as class I transposable elements, retrotransposons **(Supplementary Figure 1B)**. Importantly, PM02 encodes for 9,630 proteins, a ~61 % increase from PM01 (5,992 protein coding genes). DeepLoc 2.0 predicted that most PM02 proteins localized to the cytoplasm and nucleus with a large quantity predicted to be extracellular **(Supplementary Figure 1C)**. Consistent with this, SignalP v6.0 predicted that PM02 secreted 492 proteins, and of those, 163 were predicted to be effectors, a 7 % and 176 % increase, respectively, from PM01 **(Figure 1C) (Telenko, et al., 2020; Sperschneider J and Dodds, 2022; Teufel et al., 2022)**. This study increased contiguity, completeness, and accuracy of annotation of the *P. maydis* genome.

### Mating-Type Genes Suggest *P. maydis* is Heterothallic

113 The genes responsible for sexual reproduction are highly conserved among fungi and are often found in a
114 mating-type *(mat)* locus **(Fraser and Heitman, 2003; Ni et al., 2011)**. The *mat* locus often encodes for the
115 Anaphase-promoting complex subunit 5 (*apc5)*, cytochrome c oxidase subunit 13 (*cox13)*, endonuclease /
116 DNA lyase (*apn2),* and early endocytic patch protein (*sla2)* genes, which flank the *mat1-1*, an alpha-box
117 transcription factor, and / or the *mat1-2*, a high mobility group (HMG) transcription factor **(Figure 1D)**. Generally,
118 homothallic fungi possess both *mat1-1* and *mat1-2* idiomorphs, allowing a single cell to sexually reproduce,
119 whereas heterothallic fungi only possess one of either *mat1-1* or *mat1-2*, requiring an interaction between
120 opposite mating-types to sexually reproduce **(Ni et al., 2011)**.

121 Initial identification of the *mat* locus suggested that PM02 possessed *mat1-2*, but lacked *mat1-1*.
122 Interestingly, closely related *Colletotrichum* spp*.* possess *mat1-2* and lack *mat1-1* but are still able to sexually
123 reproduce **(Wilson et al., 2021)**. To explore whether *P. maydis* might also lack *mat1-1*, we aligned our raw
124 nanopore reads to the PM02 *mat* locus. Interestingly, we observed a ~50 % reduction in read similarity
125 precisely at the site of the *mat1-2* idiomorph **(Figure 1D)**. Following generation of a consensus sequence from
126 the reads that differed at the site of *mat1-2*, BlastX confirmed the presence of the PM02 *mat1-1* idiomorph,
127 confirming that the idiomorphs reside at the same genomic location between mating types. Since our genomic
128 reads were generated from conidial DNA isolated from several tar spots, we mapped our Illumina reads to both
129 *mat* idiomorphs to determine the ratio of mating types within our population. Our results show a near equal
130 mapping of Illumina reads to both *mat* genes, and the quantity of reads that mapped to both *mat* genes are
131 roughly half the number of reads that mapped to the neighboring *apn2* and *sla2* genes **(Figure 1E)**. This
132 confirms that *mat1-1* and *mat1-2* idiomorphs exist at a near equal ratio in our sampled population.

133 The expression of either *mat1-1* or *mat1-2* controls the downstream expression of specific pheromone
134 precursor and receptor genes required for mate recognition and subsequent sexual reproduction **(Jones and**
135 **Bennett, 2011)**. We confirmed the presence of both α- and a-factor precursor pheromone genes **(Figure 1F)**,
136 as well as both α- and a-factor receptor genes *(preA* and *preB)* **(Figure 1G)**. Together, these results suggest
137 that *P. maydis* is heterothallic, uses a pheromone precursor / receptor mechanism for mate recognition, and
138 that both mating types existed in near equal ratio within our population sampled. Further study to determine
139 whether a single tar spot lesion represents a single mating type or equal ratio of both mating types would allow
140 us to determine if sexual reproduction is uncommon or a requirement for lesion formation, respectively.
141
142
143 **Degradation of Inorganic Nitrogen Utilization Pathways**
144
145 In obligate fungal pathogens, gene loss is a common consequence of genetic drift, which can ultimately result
146 in metabolic pathway degradation or destruction **(Spanu, 2012)**. To determine if gene loss had occurred in *P.*
147 *maydis*, we first used KEGG GhostKoala to assign a K-number to each PM02 protein homolog **(Kanehisa et**
148 **al., 2016)**. In total, 812 K-numbers were assigned to PM02. Next, we collected all available K-numbers from
149 each Sordariomycete within the KEGG database and generated a presence / absence metric in relation to
150 PM02 **(Figure 2A)**. Specifically, we focused on K-numbers that were present in all Sordariomycetes, suggesting

151 an important or essential function, but that were absent in PM02. In total, we found 35 genes that fit this criterion
152 **(Supplementary Table 1)**.
153 Most notably from this analysis, we discovered severe gene loss and pathway degradation for the
154 ability of *P. maydis* to utilize inorganic nitrogen. Indeed, we found that PM02 lacked the high-affinity NrtA and
155 NrtB nitrate / nitrite transporters, nitrate reductase (NiaD), nitrilase (Nit), and formamidase (FmdA) **(Figure 2B)**.
156 Similarly, while we found that PM02 does possess a nitrite transporter (NitA), no obvious nitrite reductase
157 (NiiA) homolog was identified. This suggests that NitA might function instead as a nitrite exporter, a function
158 that has been observed in *Aspergillus nidulans* **(Akhtar et al., 2015)**. In support of this, we found both genes
159 necessary for nitroalkane utilization, 2-Nitropropane dioxygenase (NMO) and nitroalkane oxidase (NOX), are
160 present in PM02. In *Magnaporthe oryzae*, these genes combat the reactive nitrogen species that are generated
161 following colonization and subsequent triggering of host immunity by catalyzing the oxidative denitrification of
162 toxic nitroalkanes into nitrite **(Zhao et al., 2020)**. Thus, these genes likely have a similar function in *P. maydis,*
163 and the resulting nitrite is exported by NitA.
164 Interestingly, loss of inorganic nitrogen uptake and assimilation genes have also been described in
165 other obligate fungi, such as rusts **(Spanu, 2012)**. Indeed, in *Melampsora larici-populina*, which causes poplar
166 leaf rust, and in *Puccinia graminis f. sp. tritici*, which causes wheat and barley stem rust, nitrate / nitrite
167 transporters and nitrite reductase have been lost **(Duplessis et al., 2011)**. Similarly, gene loss in inorganic
168 nitrogen and sulfur assimilation pathways have also been observed in the obligate oomycete
169 *Hyaloperonospora arabidopsidis* **(Baxter et al., 2010)**. However, we found no evidence that *P. maydis* is
170 deficient in sulfur assimilation.
171
172
173 **Tar Spot Transcriptome – Carbon and Nitrogen Utilization**
174
175 Our ability to study *P. maydis* in detail is largely limited due to its obligate nature and it being recalcitrant to
176 culture. By utilizing trap plants placed into a corn field with heavy tar spot disease pressure we were able to
177 generate plants that were primarily infected with *P. maydis* with little to no other pathogens. The *P. maydis*
178 stroma lesions sampled ranged in size up to 2 mm and were no older than 24 days. Since *P. maydis* stroma
179 develop into a complex mixture of different *P. maydis* cell types as they age, it is not yet obvious how RNA-
180 seq differential reads could be disentangled and attributed to certain cell types. Therefore, we focused our
181 current efforts on profiling the transcriptome of a single timepoint, primary tar spot lesion formation. While a
182 single time point can have limitations for interpreting dynamic biological pathways, they can still be informative
183 for determining factors important for a given pathway or for what direction a given pathway is being driven at
184 our sampling time point. We also verified that these patterns were consistent across biological samples, as
185 each tar spot lesion represents a different expression profile. Our analysis revealed the relative expression
186 profile of this single timepoint, and we hypothesize upon the metabolic pathways being expressed.
187 For each metabolic pathway of *P. maydis*, we generated an average Transcripts Per Kilobase Million
188 (TPM) score, which is derived from the cumulative average expression (TPM) of each KEGG K-number-

189 associated gene within that pathway **(Supplementary Table 2)**. Following this analysis, we found that carbon
190 utilization, primarily oxidative phosphorylation (TPM = 450.84), glycolysis (TPM = 259.44), and the citric acid
191 cycle (TPM = 193.91), were in the top five highest expressed metabolic pathways **(Figure 3A and**
192 **Supplementary Figure 2A)**. Importantly, this confirms that cells within our time point were metabolically active.
193 Interestingly, we found that the nitrogen metabolic pathway was one of the highest expressed pathways (TPM
194 = 212.76), a surprising result given our previous finding that *P. maydis* had extensive gene loss in inorganic
195 nitrogen assimilation pathways **(Figures 2B and 3A)**. However, while most fungi can assimilate nitrate and
196 nitrite compounds abundant in soil, the reduction of nitrate / nitrite into ammonium is a less-preferred energy-
197 consuming process **(Campbell and Kinghorn, 1990; Crawford and Arst, 1993)**. Instead, glutamine, glutamate,
198 and / or ammonium are much more favorable sources of nitrogen, and glutamine is one of the most abundant
199 amino acids in corn, serving as a major molecule for nitrogen transport throughout tissues **(Chapman and**
200 **Leech, 1979; Magalhães et al., 1990)** In fact, corn leaves have been shown to exhibit constant glutamine
201 synthetase activity throughout leaf age and development **(Hirel et al., 2005)**, and glutamine quantification has
202 even been proposed for predicting end of season corn grain yields **(Goron et al., 2017)**, whereas other crop
203 species have shown a reduction in glutamine synthetase activity in older leaves **(Kamachi et al., 1991;**
204 **Masclaux et al., 2000; Kichey et al., 2005)**. Importantly, extensive work has demonstrated that glutamine is the
205 main marker for cellular nitrogen status in filamentous fungi **(Caddick et al., 1994; Magasanik and Kaiser, 2002;**
206 **Berger et al., 2008)**. Thus, we explored whether *P. maydis* might be utilizing glutamine, glutamate, and / or
207 ammonium as its primary nitrogen source.

208 We found that the highest expressed genes within the nitrogen assimilation pathway were glutamine
209 synthetase (Gln-1) (TPM = 1028.53), which produces glutamine from glutamate and ammonia **(Minehart and**
210 **Magasanik, 1992)**, and glutamine-fructose-6-phosphate transaminase (GfpT) (TPM = 350.32), which produces
211 D-glucosamine 6-phosphate from L-glutamine + D-fructose 6-phosphate and regulates chitin synthesis by
212 controlling glucose flux into the hexosamine pathway **(Maia, 1994) (Supplementary Figure 2B)**. Similarly, we
213 found that NAD-dependent glutamate dehydrogenase (NAD-GDH), which catalyzes glutamate from α-
214 ketoglutarate and ammonia **(Kinghorn and Pateman, 1976)**, was another highly expressed gene within the
215 pathway (TPM = 346.05), and that *P. maydis* surprisingly lacked a NADP-dependent glutamate dehydrogenase
216 (NADH-GDH), which is conserved among other Sordariomycetes within the KEGG database **(Supplementary**
217 **Figure 2B)**. While we found that the major nitrate / nitrite transporters NrtA and NrtB are missing in *P. maydis*
218 **(Figure 2B)**, we found that homologs of the *Fusarium fujikuroi* ammonium transporters MEP1 and MEP2, and
219 the glutamine specific transporter GAP, were conserved, and that expression of GAP (TPM = 257.04) was
220 much higher than either MEP1 (TPM = 90.55) or MEP2 (TPM = 75.99) **(Pfannmüller et al., 2017)**. Alternatively,
221 we observed much lower expression for the nitrate-specific transcription factors NirA and AreA **(Supplementary**
222 **Figure 2B)**, which traditionally activate inorganic nitrogen assimilation pathways in the absence of glutamine
223 and ammonium and likely have an alternate function in *P. maydis*, given the absence of this pathway **(Berger**
224 **et al., 2006; Tudzynski, 2014)**. Collectively, our results strongly suggest that *P. maydis* is utilizing ammonium,
225 glutamate, and glutamine as its primary nitrogen sources, and may offer some hints to artificial culturing of *P.*
226 *maydis*.

227

228

229 **Tar Spot Transcriptome – DNA Replication, Cell Division, and Autophagy**

230

231 When analyzing the average expression values for pathways, we were surprised to find that among pathways
232 with the relatively lowest expression were those involved in genetic processing, such as non-homologous end-
233 joining (TPM = 34.96), base excision repair (TPM = 35.22), DNA replication (TPM = 41.79), mismatch repair
234 (TPM = 46.76), homologous recombination (TPM = 61.15), and nucleotide excision repair (TPM = 65.78), as
235 well as those involved in cellular processes, such as cell cycle regulation (TPM = 93.60) and meiosis (TPM =
236 108.07) **(Figure 3B)**. Among critical genes within the DNA replication pathway with the lowest expression were:
237 (i) subunits of DNA polymerase α (PolA2 TPM = 15.78), δ (PolD3 TPM = 29.46), and ε (PolE1 TPM = 7.15,
238 PolE2 TPM = 13.69), (ii) DNA ligase 1 (TPM = 15.22), (iii) replication factor C (TPM = 17.57), (iv) flap
239 endonuclease-1 (TPM = 18.68), (v) DNA helicase (TPM = 18.88), (vi) DNA primase (TPM = 19.34), and (vii)
240 replication factor A1 (TPM = 23.26). Likewise, we also observed low expression for mcm2 (TPM = 30.08),
241 mcm3 (TPM = 14.98), mcm4 (TPM = 23.69), and mcm6 (TPM = 13.12), which are genes required for regulating
242 replication initiation in the meiotic cycle **(Lindner et al., 2002) (Supplementary Figure 2C)**. Similarly, among
243 critical genes within cell cycle regulation and meiosis with the lowest expression were: (i) anaphase-promoting
244 complex subunit 1 (TPM = 3.16), subunit 2 (TPM = 4.52), subunit 4 (TPM = 24.93), and subunit 6 (TPM =
245 17.72), which regulate mitotic progression and subsequent exit **(Chou et al., 2011)**, (ii) CDC7 (TPM = 3.80), a
246 key regulator in the initiation of DNA replication **(Masai and Arai, 2002)**, (iii) separase Esp1 (TPM = 3.94),
247 which is required for anaphase spindle elongation **(Baskerville et al., 2008)**, (iv) Swi6 (TPM = 9.66), which
248 regulates meiotic initiation **(Purnapatre et al., 2002)**, (v) Cdc45 (TPM = 25.93), which is involved in the initiation
249 and elongation steps of DNA replication **(Aparicio et al., 1999)**, (vi) Rec8 (TPM = 24.05), which is critical for
250 recombination between homologous chromosomes during meiosis **(Petronczki et al., 2003)**, (vii) Cdc6 (TPM
251 = 28.48), which is essential for initiation of DNA replication **(Cocker et al., 1996)**, and (viii) Bub1 (TPM = 38.67),
252 which is required for sister kinetochore unification and centromeric cohesion retention during the first stage of
253 meiosis **(Bernard et al., 2001) (Supplementary Figure 2D)**.

254 These findings suggest that *P. maydis* might be rerouting energy derived from plant tissues away from
255 DNA replication and cell division and towards other cellular processes, such as those involved in virulence,
256 during tar spot lesion formation. In further support of this hypothesis, we found that the average expression for
257 the autophagy pathway was moderately high, a well-characterized pathway that plays a significant role in
258 pathogenicity and conidiation **(Figure 3B and Supplementary Figure 2E) (Pollack et al., 2009; Liu et al., 2012;**
259 **Liu et al., 2016)**. Indeed, among highly expressed autophagy genes previously identified as essential for
260 pathogenicity were: (i) Sec17 (TPM = 256.93), which is required for vesicle-mediated transport between the
261 endoplasmic reticulum and the golgi apparatus, and has been shown to function in formation of *Fusarium*
262 *graminearum* effector-contained extracellular vesicles during infection of corn **(Garcia-Ceron et al., 2021)**, (ii)
263 Ykt6 (TPM = 285.58), a SNARE family protein that has been proposed to function in secretion of *Colletotrichum*
264 *orbiculare* effectors **(Irieda et al., 2014)**, (iii) Pep4 (TPM = 970.46), a late state protease involved in

265 pathogenicity of *Ustilago maydis* **(Soberanes-Gutiérrez et al., 2015)**, (iv) ATG8 (TPM = 1242.65), an essential
266 factor in autophagy that has been shown to influence pathogenicity in *Beauveria bassiana*, *Cryphonectria*
267 *parasitica*, *Fusarium graminearum*, *Ustilaginoidea virens*, and *Ustilago maydis*, **(Nadal and Gold, 2010; Ying**
268 **et al., 2016; Lv et al., 2017; Shi et al., 2019; Meng et al., 2020)**, and (v) Prb1 (TPM = 1810.36), a subtilisin-like
269 protease that has been shown to be indispensable for virulence in several plant pathogens **(Shi et al., 2014;**
270 **Fu et al., 2020)**. Together, these results suggest that *P. maydis* might be rerouting energy away from growth
271 and towards pathogenicity during tar spot lesion formation.
272
273
274 **Tar Spot Transcriptome – Protein Export**
275
276 The ability for plant pathogenic fungi to cause disease requires the secretion of numerous proteins into the
277 extracellular environment. This process involves the targeting and translocation of proteins, via N-terminal
278 signal peptides, across the endoplasmic reticulum membrane into the lumen, via the Sec61 complex. Proteins
279 are then embedded into vesicles that travel through the golgi apparatus and fuse with the cell membrane,
280 resulting in surface display or secretion of proteins into the extracellular environment **(Walter et al., 1982;**
281 **Walter et al., 1984, Greenfield and High, 1999; Cross et al., 2009; Mandon et al., 2009)**. Among the cellular
282 pathways that we analyzed, we found that gene expression for the cAMP (TPM = 228.24) and RAS (TPM =
283 245.72) signaling pathways, which are important for regulating morphogenesis and virulence, were among the
284 pathways with the highest expression **(Figure 3B) (Jacob et al., 2022)**. Similarly, we found that protein
285 processing (TPM = 233.32) and protein export (TPM = 273.64) were also pathways with relatively high average
286 expression **(Figure 3B)**. Among genes within these pathways, we found that the those with the highest
287 expression were the HSPA1s (TPM = 2119.20), HSP90A (TPM = 1373.20), and BiP (TPM = 1180.38)
288 chaperones, which play critical roles in ensuring proteins are properly folded and that membrane permeability
289 of the endoplasmic reticulum is properly maintained **(Ellgaard and Helenius, 2003)**. Similarly, we found that
290 two subunits of the SEC61 complex, SEC61G (TPM = 827.21) and SEC61A (TPM = 347.14), and the signal
291 peptidase complex, SPCS1 (TPM = 372.43), SPCS2 (TPM = 263.75), SPCS3 (TPM = 352.50), and SEC11
292 (TPM = 150.50), were also highly expressed **(Meyer and Hartmann, 1997; de la Rosa et al., 2004)**.
293 SNARE family proteins mediate the final steps of vesicle docking and membrane fusion **(Jahn and**
294 **Scheller, 2006)**. Specifically, the SNARE proteins SCN1, SSO1, and SSO2, are involved in fusion of vesicles
295 at the plasma membrane **(Saloheimo and Pakula, 2011)**. While we found that expression for SNC1 (TPM =
296 1208.37) was high, expression of both SSO1 (TPM = 144.43) and SSO2 (TPM = 45.58) were much lower and
297 more similar to expression of the general fusion factor NSF1 (TPM = 130.47), which is involved in multiple
298 vesicle fusion steps. However, expression for FTT1 (TPM = 914.65) and FTT2 (TPM = 323.35), which function
299 in the last step of secretion, were much higher in comparison **(Vasara et al., 2002)**. Collectively, these results
300 suggest that protein secretion is a process highly expressed by *P. maydis* during tar spot lesion formation.
301
302

303 **Tar Spot Transcriptome – Metabolite Transporters**

304

305 In most fungi, glucose represents the main source of carbon for energy production. To better understand the
306 sugars *P. maydis* can transport, and thus metabolize, we analyzed the repertoire of sugar transporters and
307 their respective expression profiles **(Figure 4A)**. Most notably, we found that *P. maydis* encodes 6 hexose
308 transporters that share homology with *Aspergillus nidulans* hexose transporters HXTA-E, which have
309 previously been demonstrated to transport glucose, fructose, mannose, and galactose **(Reis et al., 2013)**.
310 Among these transporters, HXTA-D showed the highest expression **(Figure 4A)**. Similarly, given that sucrose
311 represents the main sugar storage molecule in plant tissues, we observed strong expression for invertase
312 (TPM = 186.76), which catalyzes the hydrolysis of sucrose into glucose and fructose, and for two surface
313 receptors that sense extracellular glucose levels, SNF3 (TPM = 158.92) and RGT2 (TPM = 315.45) **(Figure**
314 **4A) (Kim and Rodriguez, 2021)**. Given our previous finding that *P. maydis* is likely utilizing amino acids as its
315 primary nitrogen source, we identified 6 amino acid transporters, all of which were strongly expressed **(Figure**
316 **4A)**. Among those identified were the lysine-specific transporter LysP (TPM = 346.58), the glutamine-specific
317 transporter GAP (TPM = 257.04), the general amino acid transporter INDA (TPM = 250.82), the branched-
318 chain-amino-acid transaminase BAT1 (TPM = 190.17), and the proline-specific transporter PUT4 (TPM =
319 129.00) **(Bianchi et al., 2019)**. These transporters had higher expression than additional transporters we
320 identified, including those for choline, magnesium, phosphate, urea, fluoride, and boron transport **(Figure 4A)**.

321

322

323 **Tar Spot Transcriptome – Light Sensing and Reproduction**

324

325 Filamentous fungi possess several levels of protein regulation for translating environmental cues, such as light
326 intensity, light quality, and nutrient availability, into changes in gene expression. These environmentally
327 influenced changes in gene expression ultimately regulate essential processes such as asexual and sexual
328 reproduction, spore germination, vegetative growth, nutrient uptake, secondary metabolism, and pathogenicity
329 **(Reviewed in: Yu and Fischer, 2019)**. Given the obligate nature of *P. maydis*, we wanted to investigate whether
330 PM02 possessed canonical light sensing and response pathways. Moreover, given the known importance of
331 light cues for asexual and sexual reproduction in fungi, we wanted to further search for homologs of known
332 regulators of these two processes.

333 In *Neurospora crassa*, the blue light-sensing proteins White Collar-1 (WC-1) and White Collar-2 (WC-
334 2), which form the white color complex (WCC), are critical regulatory transcription factors of the fungal circadian
335 clock **(Baek et al., 2019)**. The LOV domain-containing protein VIVID (VVD) inhibits WCC activity to modulate
336 photoadaptation **(Schwerdtfeger and Linden, 2001; Schwerdtfeger and Linden, 2003; Chen et al., 2010)**. We
337 found that PM02 possessed WC-1, WC-2, and VVD, confirming the ability for *P. maydis* to sense blue-light.
338 Beyond the WCC complex, we confirmed the presence of additional light sensing homologs, including: (i) the
339 blue light / UVA sensing protein CryA, which represses sexual development under $UVA_{350\text{-}370\ nm}$ **(Bayram et**
340 **al., 2008)**, (ii) the LaeA / VE-1 / VE-2 velvet complex, which controls asexual and sexual developmental

341 pathways **(Bayram O and Braus GH, 2012)**, (iii) SilA (but not SilG), which represses sexual reproduction in the
342 presence of light **(Han et al., 2008)**, (iv) ImeB, which is required for inhibition of sexual development in the
343 presence of light and for mycotoxin production in *A. nidulans* **(Bayram et al., 2009)**, and (v) the red light-sensing
344 photoreceptor FphA, which represses sexual development in red light **(Blumenstein et al., 2005)**. Among these
345 light-sensing proteins, WC-2 had the highest expression (TPM = 163.27), ImeB (TPM = 61.47), VE-1 (TPM =
346 57.16), VVD (TPM = 44.94), WC-1 (TPM = 43.82), SilA (TPM = 35.57), FphA (TPM = 32.56), and LaeA (TPM
347 = 26.00) had relatively moderate expression, whereas VE-2 (TPM = 12.39) and CryA (TPM = 5.87) had very
348 low expression **(Figure 4BC - Blue)**.

349 Beyond light cues, fungi also have mechanisms for directly sensing other extracellular signals that
350 subsequently regulate sexual reproduction, such as nutrients and inorganic molecules. In fact, Pho85 (PhoA)
351 senses phosphate levels by phosphorylating the transcription factor Pho4 under high phosphate conditions.
352 Alternatively, in low phosphate conditions, Pho81 inhibits PhoA **(Lenburg and O'shea, 1996; Persson et al.,**
353 **2003; Huang et al., 2007)**. LsdA, which is required for inhibiting sexual reproduction under high salt conditions,
354 is highly expressed in late sexual development **(Lee at al., 2001)**. When levels of amino acids are high, CpcB
355 promotes sexual reproduction, completion of sexual fruiting, and ascospore maturation **(Kong et al., 2013)**.
356 Finally, EsdC, which is required for early sexual development, contains a glycogen binding domain that is
357 proposed to link sexual development to nutrient availability **(Han et al., 2008; Dyer and O'Gormon, 2012)**. We
358 found homologs for PhoA, LsdA, CpcB, and EsdC in *P. maydis*, suggesting a conserved role in development
359 as in other fungi **(Figure 4C - Red)**.

360 Interestingly, among these proteins, we observed extremely high expression for EsdC (TPM =
361 6699.95), a gene whose expression was the seventh highest in our data set, which suggests that *P. maydis*
362 might have initiated or completed sexual reproduction at our timepoint sampled **(Han et al., 2008; Dyer and**
363 **O'Gormon, 2012)**. Likewise, the observed high expression for LsdA (TPM = 637.27) also suggests that sexual
364 development might have initiated or completed, since LsdA transcripts accumulate early in the sexual
365 development stage and peak in the late stage **(Figure 4C - Red) (Lee et al., 2001)**. Further supporting that
366 sexual reproduction might have initiated or completed, we found that both a-factor (TPM = 21.58) and α-factor
367 (TPM = 28.46) pheromone precursors, both PreA (TPM = 73.97) and PreB (TPM = 63.52) pheromone
368 receptors, and Mat1-1 (TPM = 71.38) and Mat1-2 (TPM = 78.93) genes were expressed, and all had relatively
369 similar expression levels between mating types **(Figure 4C - Purple)**. Lastly, consistent with our hypothesis
370 that *P. maydis* is likely utilizing amino acids as its primary source of nitrogen, expression for CpcB, which
371 promotes sexual reproduction, completion of sexual fruiting, and ascospore maturation when levels of amino
372 acids are elevated, was very high (TPM = 1087.68), a result that further suggests levels of amino acids are
373 high in tar spot lesions and that sexual reproduction might have initiated or completed **(Figure 4C - Red) (Kong**
374 **et al., 2013)**. Collectively, these results strongly suggest that sexual reproduction might occur early in tar spot
375 lesion formation. In support of this hypothesis, we observed that tar spot lesions at our sampled timepoint
376 contained multiple perithecia with asci **(Supplementary Figure 2F)**.

377 In addition to sexual reproduction, fungi can also perform asexual reproduction to generate conidia, a
378 process that has been primarily studied at the molecular level in *A. nidulans* and *N. crassa*. The fluffy genes

379 (FlbA-FlbE) are a well-studied system of proteins, activated by blue light, that initiate conidiation by activating
380 the central transcriptional regulator BrlA **(Olmedo et al., 2010; Kim et al., 2017)**. In *Aspergillus* spp., three
381 transcription factors, BrlA, AbaA, and WetA, form a central gene regulatory network that is required for the
382 development of asexual fruiting bodies **(Figure 4B) (Sewall, 1994; Alkhayyat et al., 2015)**. Interestingly, we
383 found that *P. maydis* possesses AbaA and WetA, but lacks BrlA and FluG (an alternative BrlA activator) **(Figure**
384 **4C)**. However, while FluG, AbaA, and WetA are found in *N. crassa*, no homolog of BrlA has been identified to
385 date **(Ruger-Herreros and Corrochano, 2020)**. This suggests that *P. maydis* might have a BrlA-free conidiation
386 pathway that is more similar to that of *N. crassa*. Indeed, like *N. crassa*, we also found that *P. maydis* possesses
387 the genes Fluffy (Fl) and Fluffyoid (Fld), major regulators of conidiation, aconidiate-2 (Acon-2) and aconidiate-3
388 (Acon-3), regulators of Fluffy expression, Vad-5, an additional Fluffy activator, and Csp-1 and Csp-2, which
389 are required for conidial septation **(Olmedo, et al., 2010; Sun et al., 2012) (Figure 4C)**. Additionally, we
390 identified arrested development-1 (Adv1), which is required for sexual development and perithecia formation
391 **(Dekhang et al., 2017)**. Lastly, in *Aspergillus* spp., FadA stimulates cyclic AMP (cAMP)-dependent protein
392 kinase A (PkaA) activity, a process inhibited by elevated levels of FlbA, resulting in the inhibition of asexual
393 and sexual reproduction **(Roze et al., 2004)**. Interestingly, we observed relatively high expression for Adv1
394 (TPM = 471.02), a master regulator of conserved fungal development genes **(Steffens et al., 2016)**. Moreover,
395 PkaA (TPM = 534.56) and FadA (TPM = 371.68) expression was relatively high, which suggests that
396 conidiation is inhibited. Significantly however, expression for FlbA (TPM = 123.27) was also high, suggesting
397 that the FadA-PkaA signaling pathway might be inhibited via FlbA in our tar spot lesion samples, allowing
398 primary asexual and sexual reproduction to proceed **(Figure 4C)**. Consistent with this hypothesis, we also
399 observed pycnidia at our sampled time point that contained numerous conidia **(Supplementary Figure 2G)**.

400 Our data suggests that *P. maydis* sequesters significant carbon and nutrients from host tissues during
401 tar spot lesion formation **(Figure 3A)**. Initially, this energy is likely primarily utilized for hyphal growth and
402 melanization within host tissues before reaching an optimum hyphal density (surface area) for rates of nutrient
403 diffusion and acquisition. Once reached, *P. maydis* then reroutes energy expenditure away from hyphal growth
404 and towards asexual and sexual reproduction. Once completed, energy is then likely rerouted to the secretion
405 of numerous pathogenicity factors. This process could account for why individual tar spot lesions remain
406 relatively small on leaf surfaces, instead of exhibiting continuous radial growth as the season progresses. Tar
407 spot lesions that do appear to increase in size are oblong in shape and likely the result of secondary infections
408 from ascospores or conidia falling adjacent to parent tar spot lesions. In support of this hypothesis, we found
409 that genes involved in hyphal tip growth, including: the polarisome scaffolding protein Spa2 (TPM = 116.25)
410 and actin nucleation–promoting factor Bud6 (TPM = 43.66) **(Virag and Harris, 2006)**, the formin proteins Bni1
411 (TPM = 69.77) and SepA (TPM = 69.77) **(Sheu et al., 1998; Sharpless and Harris, 2002)**, Myosin-5 (TPM =
412 46.03) **(Schuchardt et al., 2005)**, and the kinesin motor protein KipA (TPM = 77.72) **(Konzack et al., 2005)**, all
413 had much lower expression values in contrast to those genes involved in early ascospore formation, such as
414 Adv1 (TPM = 471.02), CpcB (TPM = 1087.68), and EsdC (TPM = 6699.95). This proposed mechanism is
415 further supported by our finding that the average TPM values for DNA replication (TPM = 41.79), cell cycle
416 regulation (TPM = 93.60), and meiosis (TPM = 108.07) pathways were much lower in comparison to the TPM

417 values for other analyzed pathways **(Figure 3AB)**. Together, these results support a model where *P. maydis*
418 reroutes carbon flux away from hyphal growth and towards ascospore and / or conidia formation following
419 establishment of a tar spot lesion. Whether this change in strategy is permanent, can be reversed, or is cyclic
420 in nature warrants further investigation to completely understand the disease cycle of *P. maydis*.
421
422
423 **Secreted Proteins Analysis**
424
425 The interaction of fungal plant pathogens with their host requires the secretion of a wide range of proteins that
426 facilitate host recognition, infiltration, immune suppression, disease emergence, and disease progression
427 **(Girard et al., 2013)**. Traditionally, these proteins have been identified by the presence of an N-terminal signal
428 peptide and the absence of transmembrane domains. Using SignalP v6.0, we identified 492 proteins encoded
429 by PM02 that were predicted to be secreted **(Figure 1C)**. This quantity is much lower than other well-studied
430 fungal plant pathogens with broad host ranges, including *Fusarium graminearum* PH-1 (1,172 secreted
431 proteins), *Fusarium oxysporum* 5176 (1,519 secreted proteins), *Colletotrichum gloeosporioides* Nara gc5
432 (1,824 secreted proteins), *Magnaporthe oryzae* Y34 (1,703 secreted proteins), *Botrytis cinerea* B05.10 (916
433 secreted proteins), *Verticillium alfalfae* VaMs.102 (967 secreted proteins), and *Sclerotinia sclerotiorum* 1980
434 (822 secreted proteins), and is more similar to obligate / facultative fungal plant pathogens that infect a single
435 or narrow range of hosts, including *Blumeria graminis* f. sp. *hordei* DH14 (679 secreted proteins) that infects
436 barley, *Blumeria graminis* f. sp. *tritici* 96224 (511 secreted proteins) that infects wheat, *Taphrina deformans*
437 PYCC 5710 (233 secreted proteins) that infects peach and almond fruit trees, *Hemileia vastatrix* (615 secreted
438 proteins) that infects coffee, *Puccinia striiformis* f. sp. *tritici* Race 31 (687 secreted proteins) and *Puccinia*
439 *triticina* Race 77 and Race 106 (620 secreted proteins) that infect wheat, and *Ustilago hordei* 4875-4 (469
440 secreted proteins) and *Ustilago maydis* 521 (536 secreted proteins) that infect barley and maize, respectively
441 **(Presti et al., 2015; Schuster et al., 2018; Mapuranga et al., 2022)**.
442 We further analyzed the predicted secreted proteins after first removing from our data set the 163
443 effectors predicted by EffectorP v3.0 **(Figure 1C)**. From the remaining 329 secreted proteins, we found that
444 261 were conserved among other fungi, and that 68 were unique to *P. maydis*, suggesting a potential novel
445 role in corn recognition and targeted infection **(Figure 5A)**. More recently, fungal secretomes have been further
446 characterized by carbohydrate-active enzyme (CAZyme) content **(Drula et al., 2022)**. The first class of
447 CAZyme, glycoside hydrolases (GH), break down plant cell walls by hydrolyzing glycosidic bonds in complex
448 polysaccharides **(Rafiei et al., 2021)**. Among these secreted CAZymes, we found that PM02 encoded 54
449 glycoside hydrolases with moderate expression (TPM = 172.09) **(Figure 5A)**, and of those, we were able to
450 identify 11 endoglucanases (TPM = 42.65), 11 chitinases (TPM = 204.28), 8 α-amylases (TPM = 102.98), 4
451 xylanases (TPM = 48.69), and 1 xyloglucanase (TPM = 186.61), with chitinases, xyloglucanase, and α-
452 amylases exhibiting the highest average gene expression by glycoside hydrolases during tar spot lesion
453 formation. We also found that PM02 encoded 18 proteins defined as having auxiliary activities (AA), redox
454 enzymes, that we observed as having similar average expression (TPM = 196.05) to those of glycoside

455 hydrolases **(Figure 5A)**. We only identified 6 carbohydrate esterases (CE), which hydrolyze carbohydrate
456 esters, and they exhibited moderate to low average expression (TPM = 79.25) **(Figure 5A)**. Interestingly, while
457 we only identified 3 carbohydrate-binding (CB) proteins, classically defined as those that bind cellulose, we
458 observed an extremely high average expression (TPM = 695.013) for these genes. Lastly, while we did not
459 identify any known polysaccharide lyases in PM02, we did identify 2 Glycosyl Transferases (GT); however,
460 average expression for these two genes was the lowest (TPM = 36.01) among identified CAZymes.
461 The identification of only 83 predicted secreted CAZymes is in stark contrast to other pathogenic fungi.
462 Indeed, most *Fusarium* spp. and *Magnaporthe* spp. have over 600 CAZymes, *Neurospora* spp. over 400
463 CAZymes*, Puccinia* spp. around 300 CAZymes, and *Ustilago* spp. over 200 CAZymes; among those
464 characterized, most were glycoside hydrolases **(Zhao et al., 2013)**. These results suggest a significant
465 deviation of CAZyme content between *P. maydis* and other fungi. Despite this, we were able to identify several
466 candidate proteins that likely play an important role in tar spot lesion formation. Likewise, while we found that
467 the average expression for all glycoside hydrolases was modest, we note that 8 out of the top 10 expressed
468 secreted proteins in our data set were glycoside hydrolases, and of those, the most highly expressed (TPM =
469 1953.00) was a protein predicted to belong to glycoside hydrolase family 15, glucoamylase. This family of
470 glycoside hydrolases catalyzes the release of D-glucose from starch and other oligo- and polysaccharides.
471 Similarly, of the 3 carbohydrate-binding proteins we identified, one in particular, was found to have extremely
472 high expression (TPM = 1953.30) and also possess an additional internal domain predicted to belong to
473 glycoside hydrolase family 15. Taken together, these results illuminate the complement of enzymes predicted
474 to be secreted by *P. maydis* and provide early evidence for the importance of glucoamylases during tar spot
475 lesion formation.
476
477
478 **Secreted Effectors Analysis**
479
480 Fungal effectors represent a class of small (usually <300 amino acids) cysteine rich proteins that are secreted
481 via endoplasmic reticulum-golgi transport, infiltrate host plant cells, and suppress host defense responses to
482 promote colonization **(Reviewed in: Presti et al., 2015)**. Relative to corn pathogens, *Ustilago maydis* is a well-
483 studied pathogen, and several effectors have been identified and characterized. For example, the *U. maydis*
484 protein TIN2 interacts with and stabilizes the corn protein kinase ZmTTK1, thereby inducing anthocyanin
485 biosynthesis and promoting vein infiltration **(Tanaka et al., 2014)**. Another protein, RSP3, blocks the antifungal
486 activity of mannose-binding corn proteins **(Ma et al., 2018)**. A more recently identified and characterized
487 protein, ROS burst interfering protein 1 (Rip1), functions by relocating the corn protein Zmlox3 to the nucleus,
488 thereby suppressing overall corn ROS response **(Saado et al., 2022)**. Together, these studies demonstrate
489 that thorough analyses of plant fungal effectors are needed and allow for the elucidation of the molecular
490 mechanisms of host recognition, infiltration, disease emergence, and disease progression.
491 From the 163 effectors we identified in PM02, we found that 79 were conserved among other fungi
492 and that 84 were unique to *P. maydis* **(Figure 5B)**. This result is similar to what's been described for effector

493 repertoires in closely related fungal species, such as *Colletotrichum graminicola* (48 % unique effectors)
494 **(O'Connell et al., 2012)**. Among *P. maydis* effectors that we identified to be widely conserved among other
495 fungi were cutinase and endosomal P24B **(Wang et al., 2022)**, SSCR **(Atanasova et al., 2013)**, concanavalin
496 A-like lectin/glucanase **(Guyon et al., 2014)**, GAS1 **(Xue et al., 2002)**, cyanovirin-N **(Matei et al., 2011)**, alpha-
497 N-Arabinofuranosidase B **(Wu et al., 2016)**, NEP1 **(Duhan et al., 2021)**, RLPA **(Charova et al., 2020)**, EMP24
498 **(Xie et al., 2021)**, and superoxide dismutase **(Wang et al., 2021)**. When predicting localization patterns of
499 conserved PM02 effectors, most (28 %) were predicted to be apoplastic in host tissues, with 14 % predicted
500 to localize to the cytoplasm and only 7 % predicted to localize to both compartments **(Figure 5B)**. Alternatively,
501 among unique effectors, most (31 %) were predicted to be cytoplasmic, with 9 % predicted to be apoplastic
502 and 11 % predicted to localize to both compartments **(Figure 5B)**. Significantly, among all the genes within our
503 transcriptomic analysis, we were surprised to find that 5 out of the top 15 expressed genes were effectors.
504 Moreover, one unique effector had the highest overall expression (TPM = 33633.95), and an additional
505 conserved effector that had the third highest expression (TPM = 14942.27), of all genes in our data set. These
506 results help illuminate those effectors that likely have a significant role in tar spot lesion formation and that
507 warrant further investigation to elucidate their function.
508 Since *P. maydis* is an obligate pathogen, the ability to characterize secreted effectors is extremely
509 difficult and molecular tools are limited. Despite this, a recent study characterized the subcellular organization
510 of 40 putative *P. maydis* effectors, sequences and predictions that were derived from the previous PM01
511 assembly, by expressing fluorescent-fusions of these proteins in a heterologous host plant system **(Helm et**
512 **al., 2022)**. While most of these effectors localized to the nucleus and cytosol, a few were found to localize to
513 multiple compartments; one effector localized to the nucleus, nucleolus, and plasma membrane, another
514 effector localized to the nucleus and nucleolus, and an additional effector surprisingly localized to the stroma
515 of chloroplasts **(Helm et al., 2022)**. Further effector characterization, such as quantifying host immune
516 suppression, identifying host protein interacting partners, and determining the temporal / spatial aspects of
517 secretion, will improve our understanding of how *P. maydis* is able to recognize, infiltrate, and cause disease.
518 Together, our results greatly improve upon previous foundational research on tar spot of corn and significantly
519 increase our knowledge of the biological capacity of *P. maydis* by providing a new high-quality RNA-informed
520 annotated genome assembly, the first tar spot transcriptomic analysis, and the identification of several unique
521 secreted proteins and effectors.
522
523
524 ## Acknowledgements
525
526 Partial support for this work was provided by the Corn Marketing Program of Michigan, Project GREEEN-
527 Michigan's plant agriculture initiative, the USDA National Institute of Food and Agriculture, Hatch project
528 1025521 and Michigan AgBioResearch, and NIFA project 2022-67013-37079. This work is supported in part
529 by the National Science Foundation Research Traineeship Program (DGE-1828149) to E.M.R. We thank Dr.

Addie Thompson for providing B73 seed, Dr. Kevin Childs from MSU Genomics Core for providing guidance and expertise, and Dr. Austin G. McCoy for assistance in data analysis.

## Author Contributions

E.M.R and M.I.C conceived the project. E.M.R., J.S.M., and M.I.C. designed experiments. E.M.R. collected materials and E.M.R., J.S.M., and K.G. performed experiments. J.S.M., E.M.R., and K.G. analyzed data. J.S.M. wrote the article. All authors discussed results and edited the article.

## Materials and Methods

### Isolation of DNA and RNA

For collection of DNA, sweet corn hybrids (Triple Crown White and Triple Crown Bicolor – Burpee) were grown in the Michigan State University (MSU) Research Greenhouses. At the V8 growth stage, plants were transferred to a tar spot infested field at the MSU Plant Pathology Farm for 7 days in August 2020 to produce high levels of disease. Plants were then returned to the greenhouse. After one month of growth in the greenhouse, high levels of tar spot stroma had developed on leaves, and cirrhi exuded. Ascospores and conidia from the cirrhi were vacuum harvested from leaf surfaces onto 70 mm Whatman 1 filters. High molecular weight DNA was extracted from 100 mg desiccated spores using a modified chloroform and Qiagen genomic tip extraction procedure **(Vaillancourt & Buell, 2019)**.

For RNA, B73 v.3 corn was first grown in pots for 30 days in outdoor courtyard space (MSU Research Greenhouses) in August 2021. Plants were then transported to a tar spot infested field (MSU Plant Pathology Farm). After 10 days of exposure time, plants were then transported to a greenhouse to allow symptoms to develop. After 14 days in the greenhouse, tar spot stroma ranging from 1 to 2 mm in size were visible on the leaf surfaces. Tar spot stroma were collected by sampling leaf disks using a 5 mm diameter cork borer. Five leaf disks were collected from tar spot stroma in the middle of eighth leaf. Three replicates were sampled from three separate plants, all at V8 stage. Disks were placed in FastPrep tubes and flash frozen in liquid nitrogen, followed by storage in a -80□ C freezer. Samples were prepared for extraction by addition of 1 ml RNA later ICE Tissue Transition Solution (Invitrogen). Leaf disks were lysed using Lysing Matrix A tubes (MPBio) containing 450 µl of RLC buffer (Qiagen RNeasy Plant Mini Kit) with a fast prep homogenizer (Level 5, 30 seconds). RNA was finally isolated using RNeasy Plant Mini Kit (Qiagen). Samples were then treated with DNase (Invitrogen – TURBO DNA-free).

### Genome Sequencing and Assembly

High molecular weight DNA was sent to the MSU Genomics Core for library preparation and sequencing. The ONT SQK-LSK109 Ligation Sequencing Kit was used for library preparation, and sequencing was performed on two independent PromethION FLO-PRO002 flow cells. Guppy v5.0.16 was used for base calling. In total, 7,939,416 total reads were produced with an N50 value of 9,970 and mean quality Phred score of 12.8. ONT adaptors were removed using Porechop v0.2.4 (https://github.com/rrwick/Porechop). Reads were filtered by quality 10 and length 15,000 using Nanofilt v2.6.0 **(De Coster et al., 2018)**. De-novo assembly was performed with Flye v2.9. **(Kolmogorov et al., 2019)**. Average coverage across resulting contigs was 112. Four iterations of polishing were performed with Racon v1.4.3 (https://github.com/isovic/racon). Consensus sequence was generated using Medaka v1.5.0 (https://github.com/nanoporetech/medaka).

For error-correction, Illumina sequencing was performed by the MSU Genomics Core using the same DNA. Samples were prepared using an Illumina TruSeq Nano DNA library prep kit and sequencing was performed with a NovaSeq 6000 S4 flow cell. In total, 259,624,387 paired-end reads were generated. Adapters were removed from Illumina 150 bp paired end reads with cutadapt v3.4 (https://github.com/marcelm/cutadapt). Four iterations of minimap2 v2.24 alignments **(Li, 2018)** and pilon v1.24 (https://github.com/broadinstitute/pilon) variant calling were used to polish the ONT assembly. Contigs were checked for continuity and scaffolding performed with LASTZ v1.04.15 (https://github.com/lastz/lastz). BlastX **(https://blast.ncbi.nlm.nih.gov)** was used to remove contaminating contigs. The completeness and contiguity of the assembly was assessed using BUSCO v5.3.2 using the fungal database **(Manni et al., 2021)**. Transposable elements were annotated using Extensive de-novo TE Annotator (EDTA) **(Ou et al., 2019)**. Genome size was predicted by k-mer analysis of Illumina reads with Jellyfish v.2.3.0 **(Marcais and Kingsford, 2011)** and Genome Scope (github.com/schatzlab/genomescope).

**RNA sequencing, genome annotation, and expression analysis**

RNA libraries and sequencing was performed at the MSU Genomics Core. Paired end 150 bp libraries were prepared with stranded mRNA Illumina TruSeq ligation kit and sequencing performed with an Illumina NovaSeq 6000 S4 flow cell. In total, 121,178,185 paired-end reads were generated for rep 1, 129,677,772 paired-end reads were generated for rep 2, and 110,704,703 paired-end reads were generated for rep 3. Raw reads were processed using cutadapt v3.4 **(Martin, 2011)**. Corn reads were removed by alignment to the B73 v.5 genome with HISAT2 v2.2.1 **(Kim et al., 2019)** and filtered with SAMtools v1.15.1 **(Danecek et al., 2009)**. The resulting unmapped reads from the three reps were concatenated and aligned to our polished *P. maydis* genome assembly with HISAT2 v2.2.1 **(Kim et al., 2019)**. This alignment was used by BRAKER2 v2.1.6 --fungus for genome annotation default settings **(Stanke et al., 2006, 2008; Hoff et al., 2016, 2019; Bruna et al., 2021)**. Functional gene assignments were performed with PANNZER2 web server **(Törönen and Holm, 2021)**. CAZyme prediction was performed with dbCAN meta server (https://bcb.unl.edu/dbCAN2/). Signal peptides and localization patterns were predicted using SignalP v6.0 and DeepLoc v2.0 respectively **(Teufel et al., 2022; Thumuluri et al., 2021)**. Effectors were predicted from the predicted secreted proteins using EffectorP v3.0 **(Sperschneider and Dodds, 2022)**. For analysis of gene expression, the three independent replicates were

individually aligned to our *P. maydis* annotated assembly using HISAT2 v2.2.1 **(Kim et al., 2019)**. StringTie v2.2.1 was then utilized to calculate FPKM and TPM values for each gene **(Pertea et al., 2016)**. Transcriptome analyses was conducted in RStudio v4.2.0 using the tidyverse v1.3.1 **(Wickham et al., 2019)** and cowplot v1.1.1 (https://github.com/wilkelab/cowplot/) packages.

## Data Availability

PM02 genome assembly, annotation, mitochondrial genome, and raw sequence data can be found under NCBI BioProject PRJNA928553.

617

618 ## References

619

620 Akhtar N, Karabika E, Kinghorn JR, Glass ADM, Unkles SE, and Rouch DA. 2015. High-affinity nitrate/nitrite
621 transporters NrtA and NrtB of *Aspergillus nidulans* exhibit high specificity and different inhibitor sensitivity.
622 *Microbiology (Reading)*. 161(Pt 7): 1435–1446.

623

624 Alkhayyat F, Kim SC, and Yu J-H. 2015. Genetic control of asexual development in *Aspergillus fumigatus*. *Adv*
625 *Appl Microbiol*. 90:93-107.

626

627 Aparicio OM, Stout AM, and Bell SP. 1999. Differential assembly of Cdc45p and DNA polymerases at early
628 and late origins of DNA replication. *Proc Natl Acad Sci USA*. 96(16):9130-5.

629

630 Atanasova L, Crom SL, Gruber S, Coulpier F, Seidl-Seiboth V, Kubicek CP, and Druzhinina IS. 2013.
631 Comparative transcriptomics reveals different strategies of *Trichoderma mycoparasitism*. *BMC Genomics*. 14:
632 121.

633

634 Baek M, Virgilio S, Lamb TM, Ibarra O, Andrade JM, Gonçalves RD, Dovzhenok A, Lim S, Bell-Pedersen D,
635 Bertolini MC, et al. 2019. Circadian clock regulation of the glycogen synthase (gsn) gene by WCC is critical for
636 rhythmic glycogen metabolism in *Neurospora crassa*. *Proc Natl Acad Sci USA*. 116, 10435–10440.

637

638 Baskerville C, Segal M, and Reed SI. 2008. The protease activity of yeast separase (Esp1) is required for
639 anaphase spindle elongation independently of its role in cleavage of cohesin. *Genetics*. 178(4): 2361–2372.

640

641 Baxter L, Tripathy S, Ishaque N, Boot N, Cabral A, Kemen E, Thines M, et al. 2010. Signatures of adaptation
642 to obligate biotrophy in the *Hyaloperonospora arabidopsidis* genome. *Science*. 330(6010): 1549–1551.

643

644 Bayram Ö, Biesemann C, Krappmann S, Galland P, and Braus GH. 2008. More than a repair enzyme:
645 *Aspergillus nidulans* photolyase-like CryA is a regulator of sexual development. *Mol Biol Cell*. 19(8): 3254–
646 3262.

647

648 Bayram Ö, Sari F, Braus GH, and Irniger S. 2009. The protein kinase ImeB is required for light-mediated
649 inhibition of sexual development and for mycotoxin production in *Aspergillus nidulans*. *Mol Microbiol*.
650 71(5):1278-95.

651

652 Bayram Ö and Braus GH. 2012. Coordination of secondary metabolism and development in fungi: the velvet
653 family of regulatory proteins. *FEMS Microbiol Rev*. 36(1):1-24.

654

Berger H, Pachlinger R, Morozov I, Goller S, Narendja F, Caddick M, and Strauss J. 2006. The GATA factor AreA regulates localization and in vivo binding site occupancy of the nitrate activator NirA. *Mol Microbiol*. 59(2):433-46.

Berger H, Basheer A, Böck S, Reyes-Dominguez Y, Dalik T, Altmann F, and Strauss J. 2008. Dissecting individual steps of nitrogen transcription factor cooperation in the *Aspergillus nidulans* nitrate cluster. *Mol Microbiol*. 69(6):1385-98.

Bernard P, Maure JF, and Javerzat JP. 2001. Fission yeast Bub1 is essential in setting up the meiotic pattern of chromosome segregation. *Nat Cell Biol*. 3(5):522-6.

Bianchi F, van't Klooster JS, Ruiz SJ, and Poolman B. 2019. Regulation of amino acid transport in *Saccharomyces cerevisiae*. *Microbiol Mol Biol Rev*. 83(4): e00024-19.

Blumenstein A, Vienken K, Tasler R, Purschwitz J, Veith D, Frankenberg-Dinkel N, and Fischer R. 2005. The *Aspergillus nidulans* phytochrome FphA represses sexual development in red light. *Curr Biol*. 15(20):1833-8.

Both M, Csukai M, Stumpf MPH, and Spanua PD. 2005. Gene expression profiles of *Blumeria graminis* indicate dynamic changes to primary metabolism during development of an obligate biotrophic pathogen. *Plant Cell*. 17(7): 2107–2122.

Brůna T, Hoff KJ, Lomsadze A, Stanke M, and Borodovsky M. 2021. BRAKER2: automatic eukaryotic genome annotation with GeneMark-EP+ and AUGUSTUS supported by a protein database. *NAR Genom Bioinform*. 3(1): lqaa108.

Breunig M, Bittner R, Dolezal A, Ramcharan A, Bunkers G. 2023. An assay to reliably achieve Tar Spot symptoms on corn in a controlled environment. *BioRxiv.* doi: 10.1101/2023.01.12.523803

Caddick MX, Peters D, and Platt A. 1994. Nitrogen regulation in fungi. *Antonie Van Leeuwenhoek*. 65(3):169-77.

Campbell WH and Kinghorn KR. 1990. Functional domains of assimilatory nitrate reductases and nitrite reductases. *Trends Biochem Sci*. 15(8):315-9.

Chapman DJ and Leech RM. 1979. Changes in pool sizes of free amino acids and amides in leaves and plastids of *Zea mays* during leaf development. *Plant Physio*l. 63, 567–572.

692 Charova SN, Dölfors F, Holmquist L, Moschou PN, Dixelius C, and Tzelepis G. 2020. The RsRlpA effector is
693 a protease inhibitor promoting *Rhizoctonia solani* virulence through suppression of the hypersensitive
694 response. *Int J Mol Sci*. 21(21): 8070.
695
696 Chen C-H, DeMay BS, Gladfelter AS, Dunlap JC, and Loros JJ. 2010. Physical interaction between VIVID and
697 white collar complex regulates photoadaptation in *Neurospora*. *Proc Natl Acad Sci USA*. 107(38):16715-20.
698
699 Chou H, Glory A, and Bachewich C. 2011. Orthologues of the anaphase-promoting complex/cyclosome
700 coactivators Cdc20p and Cdh1p are important for mitotic progression and morphogenesis in *Candida albicans*.
701 *Eukaryot Cell*. 10(5): 696–709.
702
703 Cocker JH, Piatti S, Santocanale S, Nasmyth K, and Diffley JF. 1996. An essential role for the Cdc6 protein in
704 forming the pre-replicative complexes of budding yeast. *Nature*. 379(6561):180-2.
705
706 Crawford NM and Arst Jr HN. 1993. The molecular genetics of nitrate assimilation in fungi and plants. *Annu*
707 *Rev Genet*. 27:115-46.
708
709 Cross BC, Sinning I, Luirink J. and High S. 2009. Delivering proteins for export from the cytosol. *Nat Rev Mol*
710 *Cell Biol*. 10, 255–264.
711
712 Danecek P, Bonfield JK, Liddle J, Marshall J, Ohan V, Pollard MO, et al. 2021. Twelve years of SAMtools and
713 BCFtools. *Gigascience*. 10(2):giab008.
714
715 Dekhang R, Wu C, Smith KM, Lamb TM, Peterson M, Bredeweg EL, et al. 2017. The *Neurospora* transcription
716 factor ADV-1 transduces light signals and temporal information to control rhythmic expression of genes
717 involved in cell fusion. *G3* (Bethesda). 7(1): 129–142.
718
719 de la Rosa JM, Ruiz T, Fonzi WA, and Rodríguez L. 2004. Analysis of heterologous expression of *Candida*
720 *albicans* SEC61 gene reveals differences in Sec61p homologues related to species-specific functionality.
721 *Fungal Genet Biol*. 41(10):941-53.
722
723 De Coster W, D'Hert S, Schultz DT, Cruts M, and Broeckhoven CV. 2018. NanoPack: visualizing and
724 processing long-read sequencing data. *Bioinformatics*. 34(15):2666-2669.
725
726 da Silva CR, Check J, MacCready JS, Alakonya AE, Beiriger R, et al. 2021. Recovery plan for tar spot of corn,
727 caused by *Phyllachora maydis*. *Plant Health Prog*. 22, 596– 616.
728

729 Drula E, Garron M-L, Dogan S, Lombard V, Henrissat B, and Terrapon N. 2022. The carbohydrate-active
730 enzyme database: functions and literature. *Nucleic Acids Res*. 50(D1):D571-D577.
731
732 Duhan D, Gajbhiye S, Jaswal R, Singh RP, Sharma TR, and Rajarammohan S. 2021. Functional
733 characterization of the Nep1-Like protein effectors of the necrotrophic pathogen – *Alternaria brassicae*. *Front*
734 *Microbiol*. 12: 738617.
735
736 Duplessis S, Cuomo CA, Lin Y-C, Aerts A, Tisserant E, Veneault-Fourrey C, Joly DL, Hacquard S, et al. 2011.
737 Obligate biotrophy features unraveled by the genomic analysis of rust fungi. *Proc Natl Acad Sci USA*.
738 108(22):9166-71.
739
740 Dyer PS and O'Gorman CM. 2012. Sexual development and cryptic sexuality in fungi: insights from *Aspergillus*
741 species. *FEMS Microbiol Rev*. 36(1):165-92.
742
743 Ellgaard L and Helenius A. 2003. Quality control in the endoplasmic reticulum. *Nat Rev Mol Cell Biol*. 4, 181–
744 191.
745
746 Fraser JA and Heitman J. 2003. Fungal mating-type loci. *Curr Biol*. 13(20):R792-5.
747
748 Fu H, Chung K-R, Liu X, Li H. 2020. Aaprb1, a subtilsin-like protease, required for autophagy and virulence of
749 the tangerine pathotype of *Alternaria alternata*. *Microbiol Res*. 240:126537.
750
751 Garcia-Ceron D, Lowe RGT, McKenna JA, Brain LM, Dawson CS, Clark B, Berkowitz O, Faou P, Whelan J,
752 Bleackley MR, and Anderson MA. 2021. Extracellular Vesicles from *Fusarium graminearum* Contain Protein
753 Effectors Expressed during Infection of Corn. *J Fungi (Basel)*. 7(11): 977.
754
755 Girard V, Dieryckx C, Job C, and Job D. 2013. Secretomes: the fungal strike force. *Proteomics*. 13(3-4):597-
756 608.
757
758 Goron T, Nederend J, Stewart G, Deen B, and Raizada M. 2017. Mid-season leaf glutamine predicts end-
759 season maize grain yield and nitrogen content in response to nitrogen fertilization under field conditions.
760 *Agronomy*. 7(2), 41.
761
762 Greenfield JJ and High S. 1999. The Sec61 complex is located in both the ER and the ER-Golgi intermediate
763 compartment. *J Cell Sci*. 112 Pt 10, 1477–1486.
764

765 Guo J, Dai X, Xu J-R, Wang Y, Bai P, Liu F, Duan Y, Zhang H, Huang L, and Kang Z. 2011. Molecular
766 Characterization of a Fus3/Kss1 Type MAPK from *Puccinia striiformis* f. sp. *tritici*, PsMAPK1. *PLoS One*. 6(7):
767 e21895.
768
769 Guyon K, Balagué C, Roby D, and Raffaele S. 2014. Secretome analysis reveals effector candidates
770 associated with broad host range necrotrophy in the fungal plant pathogen *Sclerotinia sclerotiorum*. *BMC*
771 *Genomics*. 15(1): 336.
772
773 Han K-H, Kim J-H, Moon H, Kim S, Lee S-S, Han D-M, Jahng K-Y, Chae KS. 2008. The *Aspergillus nidulans*
774 esdC (early sexual development) gene is necessary for sexual development and is controlled by veA and a
775 heterotrimeric G protein. *Fungal Genet Biol*. 45(3):310-8.
776
777 Han SY, Ko JA, Kim JH, Han KY, Han KH, and Han DM. 2008. Isolation and functional analysis of the silA
778 gene that controls sexual development in response to light in *Aspergillus nidulans*. *Kor J Mycol*. 36: 189–195.
779
780 Helm M, Singh R, Hiles RR, Jaiswal N, Myers A, Iyer-Pascuzzi AS, and Goodwin S. 2022. Candidate effector
781 proteins from the maize tar spot pathogen *Phyllachora maydis* localize to diverse plant cell compartments.
782
783 Henningsen EC, Omidvar V, Coletta RD, Michno J-M, Gilbert E, Li F, Miller ME, Myers CL, Gordon SP, Vogel
784 JP, Steffenson BJ, Kianian SF, Hirsch CD, and Figueroa M. 2021. Identification of candidate susceptibility
785 genes to *Puccinia graminis* f. sp. *tritici* in wheat. *Front Plant Sci*. 12:657796.
786
787 Hirel B, Martin A, Terce-Laforgue T, Gonzalez-Moro MB, Estavillo JM. 2005. Physiology of maize I: a
788 comprehensive and integrated view of nitrogen metabolism in a C4 plant. *Physiol Plant*. 124:167–177.
789
790 Hock J, Kranz J, and Renfo BL. 1995. Studies on the epidemiology of the tar spot disease complex of maize
791 in Mexico. *Plant Path*. 44:490-502.
792
793 Hoff KJ, Lange S, Lomsadze A, Borodovsky M, and Stanke M. 2016. BRAKER1: unsupervised RNA-Seq-
794 based genome annotation with GeneMark-ET and AUGUSTUS. *Bioinformatics*. 32(5):767-769.
795
796 Hoff KJ, Lomsadze A, Borodovsky M, and Stanke M. 2019. Whole-Genome Annotation with BRAKER.
797 *Methods Mol Biol*. 1962:65-95.
798
799 Huang K, Ferrin-O'Connell I, Zhang W, Leonard GA, O'Shea EK, and Quiocho FA. 2007. Structure of the
800 Pho85-Pho80 CDK-cyclin complex of the phosphate-responsive signal transduction pathway. *Mol Cell*.
801 28(4):614–23.
802

803 Irieda H, Maeda H, Akiyama K, Hagiwara A, Saitoh H, Uemura A, Terauchi R, and Takano Y. 2014.
804 *Colletotrichum orbiculare* secretes virulence effectors to a biotrophic interface at the primary hyphal neck via
805 exocytosis coupled with SEC22-mediated traffic. *Plant Cell*. 26(5):2265-2281.
806
807 Jacob S, Bühring S, and Bersching K. 2022. Recent advances in research on molecular mechanisms of fungal
808 signaling. *Encyclopedia*. 2(2), 840-863
809
810 Jahn R and Scheller RH. 2006. SNAREs--engines for membrane fusion. *Nat Rev Mol Cell Biol*. 7(9):631-43.
811
812 Jones SK and Bennett RJ. 2011. Fungal mating pheromones: choreographing the dating game. *Fungal Genet*
813 *Biol*. 48(7):668-76.
814
815 Kamachi K, Yamaya T, Mae T, Ojima K. 1991. A role for glutamine synthetase in the remobilization of leaf
816 nitrogen during natural senescence in rice leaves. *Plant Physiol*. 96:411–417.
817
818 Kanehisa M, Sato Y, and Morishima K. 2016. BlastKOALA and GhostKOALA: KEGG tools for functional
819 characterization of genome and metagenome sequences. *J Mol Biol*. 428, 726-731.
820
821 Kichey T, Le Gouis J, Sangwan B, Hirel B, Dubois F. 2005. Changes in the cellular and subcellular localization
822 of glutamine synthetase and glutamate dehydrogenase during flag leaf senescence in wheat (*Triticum*
823 *aestivum* L.). *Plant Cell Physiol*. 46:964–974.
824
825 Kim D, Langmead B, and Salzberg SL. 2015. HISAT: a fast spliced aligner with low memory requirements. *Nat*
826 *methods*. 12(4):357-60.
827
828 Kim YJ, Yu YM, and Maeng PJ. 2017. Differential control of asexual development and sterigmatocystin
829 biosynthesis by a novel regulator in *Aspergillus nidulans*. *Sci Rep*. 7:46340.
830
831 Kim J-H and Rodriguez R. 2021. Glucose regulation of the paralogous glucose sensing receptors Rgt2 and
832 Snf3 of the yeast *Saccharomyces cerevisiae*. *Biochim Biophys Acta Gen Subj*. 1865(6):129881.
833
834 Kinghorn JR and Pateman JA. 1976. Mutants of *Aspergillus nidulans* lacking nicotinamide adenine
835 dinucleotide-specific glutamate dehydrogenase. *J Bacteriol*. 125(1): 42–47.
836
837 Kolmogorov M, Yuan J, Lin Y, and Pevzner PA. 2019. Assembly of long, error-prone reads using repeat graphs.
838 *Nat Biotechnol*. 37(5):540-546.
839

840 Kong Q, Wang L, Liu Z, Kwon N-J, Kim SC, and Yu J-H. 2013. Gβ-like CpcB plays a crucial role for growth
841 and development of *Aspergillus nidulans* and *Aspergillus fumigatus*. *PLoS One*. 8(7):e70355.
842
843 Konzack S, Rischitor PE, Enke C, and Fischer R. 2005. The role of the kinesin motor KipA in microtubule
844 organization and polarized growth of *Aspergillus nidulans*. *Mol Biol Cell*. 16(2): 497–506.
845
846 Lanver D, Müller AN, Happel P, Schweizer G, Haas FB, Franitza M, Pellegrin C, Reissmann S, Altmüller J,
847 Rensing SA, and Kahmann R. 2018. The biotrophic development of *Ustilago maydis* studied by RNA-seq
848 analysis. *Plant Cell*. 30(2):300-323.
849
850 Lee DW, Kim S, Kim SJ, Han DM, Jahng KY, and Chae KS. 2001. The lsdA gene is necessary for sexual
851 development inhibition by a salt in *Aspergillus nidulans*. *Curr Genet*. 39(4):237-43.
852
853 Lenburg ME and O'Shea EK. 1996. Signaling phosphate starvation. *Trends Biochem Sci.* 21(10):383–7.
854
855 Li, H. 2018. Minimap2: pairwise alignment for nucleotide sequences. *Bioinformatics*. 34:3094-3100.
856
857 Lindner K, Gregán J, Montgomery S, and Kearsey SE. 2002. Essential role of MCM proteins in premeiotic
858 DNA replication. *Mol Biol Cell*. 13(2): 435–444.
859
860 Liu X-H, Gao H-M, Xu F, Lu J-P, Devenish RJ, and Lin FC. 2012. Autophagy vitalizes the pathogenicity of
861 pathogenic fungi. *Autophagy*. 8(10):1415-25.
862
863 Liu X-H, Xu F, Snyder JH, Shi H-B, Lu J-P, and Lin F-C. 2016. Autophagy in plant pathogenic fungi. *Semin*
864 *Cell Dev Biol*. 57:128-137.
865
866 Lv W, Wang C, Yang N, Que Y, Talbot NJ, and Wang Z. 2017. Genome-wide functional analysis reveals that
867 autophagy is necessary for growth, sporulation, deoxynivalenol production and virulence in *Fusarium*
868 *graminearum*. *Sci Rep*. 7(1):11062.
869
870 Ma L-S, Wang L, Trippel C, Mendoza-Mendoza A, Ullmann S, Moretti M, Carsten A, et al. 2018. The *Ustilago*
871 *maydis* repetitive effector Rsp3 blocks the antifungal activity of mannose-binding maize proteins. *Nat Commun*.
872 9(1):1711.
873
874 Magalhães JR, Ju GC, Rich PJ, and Rhodes D. 1990. Kinetics of 15NH4+ assimilation in *Zea mays*. *Plant*
875 *Physiol*. 94, 647–656.
876
877 Magasanik B and Kaiser CA. 2002. Nitrogen regulation in *Saccharomyces cerevisiae*. *Gene*. 290(1-2):1-18.

878

879 Maia JC. 1994. Hexosamine and cell wall biogenesis in the aquatic fungus *Blastocladiella emersonii*. *FASEB*
880 *J*. 8(11):848-53.
881

882 Mandon EC, Trueman SF, and Gilmore R. 2009. Translocation of proteins through the Sec61 and SecYEG
883 channels. *Curr Opin Cell Biol*. 21, 501–507.
884

885 Manni M, Berkeley MR, Seppey M, and Zdobnov EM. 2021. BUSCO: Assessing genomic data quality and
886 beyond. *Curr Protoc*. 1(12):e323.
887

888 Mapuranga J, Zhang N, Zhang L, Chang J, Yang W. 2022. Infection strategies and pathogenicity of biotrophic
889 plant fungal pathogens. *Front Microbiol*. 13:799396.
890

891 Marcais G and Kingsford C. 2011. A fast, lock-free approach for efficient parallel counting of occurrences of k-
892 mers. *Bioinformatics*. 27(6): 764-770.
893

894 Martin M. 2011. Cutadapt removes adapter sequences from high-throughput sequencing reads. *EMBnet*
895 *Journal*. 17, 10-12.
896

897 Masai H and Arai K. 2002. Cdc7 kinase complex: a key regulator in the initiation of DNA replication. *J Cell*
898 *Physiol*. 190(3):287-96.
899

900 Masclaux C, Valadier MH, Brugiere N, Morot-Gaudry JF, Hirel B. 2000. Characterization of the sink/source
901 transition in tobacco (*Nicotiana tabacum* L.) shoots in relation to nitrogen management and leaf senescence.
902 *Planta*. 211:510–518.
903

904 Matei E, Louis JM, Jee J, and Gronenborn AM. 2011. NMR solution structure of a cyanovirin homolog from
905 wheat head blight fungus. *Proteins*. 79(5): 1538–1549.
906

907 Maublanc A. 1904. Especes nouvelles de champignons inferieurs. Bull Soc Mycol Fr. 20:72-74.
908

909 Meng S, Xiong M, Jagernath JS, Wang C, Qiu J, Shi H, and Kou Y. 2020. UvAtg8-mediated autophagy
910 regulates fungal growth, stress responses, conidiation, and pathogenesis in *Ustilaginoidea virens*. *Rice* (N Y).
911 13: 56.
912

913 Meyer HA and Hartmann E. 1997. The yeast SPC22/23 homolog Spc3p is essential for signal peptidase
914 activity. *J Biol Chem*. 272(20):13159-64.
915

Minehart PL and Magasanik B. 1992. Sequence of the GLN1 gene of *Saccharomyces cerevisiae*: role of the upstream region in regulation of glutamine synthetase expression. *J Bacteriol*. 174(6):1828-36.

Mueller DS, Wise KA, Sisson AJ, Allen TW, Bergstrom GC, Bissonnette KM, et al. 2020. Corn yield loss estimates due to diseases in the United States and Ontario, Canada, from 2016 to 2019. *Plant Health Prog*. 21, 238– 247.

Mueller DS, Wise KA, and Sisson A. 2022. Corn Disease Loss Estimates From the United States and Ontario, Canada — 2021. *Crop Protection Network*. 10.31274/cpn-20220722-0.

Nadal M and Gold SE. 2010. The autophagy genes atg8 and atg1 affect morphogenesis and pathogenicity in *Ustilago maydis*. *Mol Plant Pathol*. 11(4): 463–478.

Ni M, Feretzaki M, Sun S, Wang X, and Heitman J. 2011. Sex in Fungi. *Annu Rev Genet*. 45: 405–430.

O'Connell RJ, Thon MR, Hacquard S, Amyotte SG, Kleemann J, et al. 2012. Lifestyle transitions in plant pathogenic *Colletotrichum* fungi deciphered by genome and transcriptome analyses. *Nat Genet*. 44(9):1060-5.

Olmedo M, Ruger-Herreros C, and Corrochano LM. 2010. Regulation by blue light of the fluffy gene encoding a major regulator of conidiation in *Neurospora crassa*. *Genetics*. 184(3): 651–658.

Ou S, Su W, Liao Y, Chougule K, Agda JRA, Hellinga AJ, Lugo CSB, et al. 2019. Benchmarking transposable element annotation methods for creation of a streamlined, comprehensive pipeline. *Genome Biol*. 20(1):275.

Persson BL, Lagerstedt JO, Pratt JR, Pattison-Granberg J, Lundh K, Shokrollahzadeh S, et al. 2003. Regulation of phosphate acquisition in *Saccharomyces cerevisiae*. *Curr Genet*. 43(4):225–44.

Pertea M, Kim D, Pertea GM, Leek JT, and Salzberg SL. 2016. Transcript-level expression analysis of RNA-seq experiments with HISAT, StringTie and Ballgown. *Nat Protoc*. 11(9):1650-67.

Petronczki M, Siomos MF, and Nasmyth K. 2003. Un ménage à quatre: the molecular biology of chromosome segregation in meiosis. *Cell*. 112(4):423-40.

Pfannmüller A, Boysen JM, and TudzynskiB. 2017. Nitrate assimilation in *Fusarium fujikuroi* is controlled by multiple levels of regulation. *Front Microbiol*. 8:381.

Pollack JK, Harris SD, and Marten MR. 2009. Autophagy in filamentous fungi. *Fungal Genet Biol*. 46(1):1-8.

954

955 Presti LL, Lanver D, Schweizer G, Tanaka S, Liang L, Tollot M, Zuccaro A, Reissmann S, and Kahmann R.
956 2015. Fungal effectors and plant susceptibility. *Annu Rev Plant Biol*. 66:513-45.
957

958 Purnapatre K, Piccirillo S, Schneider BL, and Honigberg SM. 2002. The CLN3/SWI6/CLN2 pathway and SNF1
959 act sequentially to regulate meiotic initiation in *Saccharomyces cerevisiae*. *Genes Cells*. 7(7):675-91.
960

961 Rafiei V, Vélëz H, and Tzelepis G. 2021. The role of glycoside hydrolases in phytopathogenic fungi and
962 oomycetes virulence. *Int J Mol Sci*. 22(17): 9359.
963

964 Reis TFD, Menino JF, Bom VLP, Brown NA, Colabardini AC, Savoldi M, Goldman MHS, Rodrigues F, and
965 Goldman GH. 2013. Identification of glucose transporters in *Aspergillus nidulans*. *PLoS One*. 8(11):e81412.
966

967 Roze LV, Beaudry RM, Keller NP, Linz JE. 2004. Regulation of aflatoxin synthesis by FadA/cAMP/protein
968 kinase A signaling in *Aspergillus parasiticus*. *Mycopathologia*. 158(2):219-32.
969

970 Ruger-Herreros C and Corrochano LM. 2020. Conidiation in *Neurospora crassa*: vegetative reproduction by a
971 model fungus. *Int Microbiol*. 23(1):97-105.
972

973 Ruhl G, Romberg MK, Bissonnette S, Plewa D, Creswell T, and Wise KA. 2016. First report of tar spot on corn
974 caused by *Phyllachora maydis* in the United States. *Plant Disease*. 100(7): 1496
975

976 Saado I, Chia K-S, Betz R, Alcântara A, Pettkó-Szandtner A, Navarrete F, D'Auria JC, Kolomiets MV, Melzer
977 M, Feussner I, and Djamei A. 2022. Effector-mediated relocalization of a maize lipoxygenase protein triggers
978 susceptibility to *Ustilago maydis*. *Plant Cell*. 34(7):2785-2805.
979

980 Saloheimo M and Pakula TM. 2011. The cargo and the transport system: secreted proteins and protein
981 secretion in *Trichoderma reesei* (*Hypocrea jecorina*). *Microbiology (Reading)*. 158(Pt 1):46-57.
982

983 Schuchardt I, Assmann D, Thines E, Schuberth C, and Steinberg G. 2005. Myosin-V, kinesin-1, and kinesin-3
984 cooperate in long-distance transport in hyphal growth of the fungus *Ustilago maydis*. *Mol Biol Cell*. 16:5191-
985 5201.
986

987 Schuster M, Schweizer G, and Kahmann R. 2018. Comparative analyses of secreted proteins in plant
988 pathogenic smut fungi and related basidiomycetes. *Fungal Genet Biol*. 112:21-30.
989

990 Schwerdtfeger C and Linden H. 2001. Blue light adaptation and desensitization of light signal transduction in
991 *Neurospora crassa*. *Mol Microbiol*. 39(4):1080-7.

992

993 Schwerdtfeger C and Linden H. 2003. VIVID is a flavoprotein and serves as a fungal blue light photoreceptor
994 for photoadaptation. *EMBO J*. 22(18):4846-55.

995

996 Sewall TC. 1994. Cellular effects of misscheduled brlA, abaA, and wetA expression in *Aspergillus nidulans*.
997 *Can J Microbiol*. 40(12):1035-42.

998

999 Sharpless KE and Harris SD. 2002. Functional characterization and localization of the *Aspergillus nidulans*
1000 formin SEPA. *Mol Biol Cell*. 13(2): 469–479.

1001

1002 Sheu YJ, Santos B, Fortin N, Costigan C, and Snyder M. 1998. Spa2p interacts with cell polarity proteins and
1003 signaling components involved in yeast cell morphogenesis. *Mol Cell Biol*. 18:4053-4069.

1004

1005 Shi L, Li R, Liao S, Bai L, Lu Q, and Chen B. 2014. Prb1, a subtilisin-like protease, is required for virulence
1006 and phenotypical traits in the chestnut blight fungus. *FEMS Microbiol Lett*. 359(1):26-33.

1007

1008 Shi L, Wang J, Quan R, Yang F, Shang J, and Chen B. 2019. CpATG8, a homolog of yeast autophagy protein
1009 ATG8, is required for pathogenesis and hypovirus accumulation in the chest blight fungus. *Front Cell Infect*
1010 *Microbiol*. 9: 222.

1011

1012 Singh J, Aggarwal R, Gurjar MS, Sharma S, Jain S, and Saharan MS. 2020. Identification and expression
1013 analysis of pathogenicity-related genes in *Tilletia indica* inciting Karnal bunt of wheat. *Australas Plant Pathol*.
1014 49:393–402.

1015

1016 Skibbe DS, Doehlemann G, Fernandes J, and Walbot V. 2010. Maize tumors caused by *Ustilago maydis*
1017 require organ-specific genes in host and pathogen. *Science*. 328(5974):89-92.

1018

1019 Soberanes-Gutiérrez CV, Juárez-Montiel M, Olguín-Rodríguez O, Hernández-Rodríguez C, 1 Ruiz-Herrera J
1020 and Villa-Tanaca L. 2015. The pep4 gene encoding proteinase A is involved in dimorphism and pathogenesis
1021 of *Ustilago maydis*. *Mol Plant Pathol*. 16(8): 837–846.

1022

1023 Spanu PD. 2012. The genomics of obligate (and nonobligate) biotrophs. *Annu Rev Phytopathol*. 50:91-109.

1024

1025 Sperschneider J and Dodds PN. 2022. EffectorP 3.0: Prediction of apoplastic and cytoplasmic effectors in fungi
1026 and oomycetes. *Mol Plant Microbe Interact*. 35(2):146-156.

1027

1028 Stanke M, Schöffmann O, Morgenstern B, and Waack S. 2006. Gene prediction in eukaryotes with a
1029 generalized hidden Markov model that uses hints from external sources. *BMC Bioinformatics*. 7:62.

1030

1031 Stanke M, Diekhans M, Baertsch R, and Haussler D. 2008. Using native and syntenically mapped cDNA
1032 alignments to improve de novo gene finding. *Bioinformatics*. 24(5):637-44.

1033

1034 Steffens EK, Becker K, Krevet S, Teichert I, and Kück U. 2016. Transcription factor PRO1 targets genes
1035 encoding conserved components of fungal developmental signaling pathways. *Mol Microbiol*. 102(5):792-809.

1036

1037 Stergiopoulos I and Wit PJGM. 2009. Fungal effector proteins. *Annu Rev Phytopathol*. 47:233-63.

1038

1039 Sun X, Yu L, Lan N, Wei S, Yu Y, Zhang H, Zhang X, and Li S. 2012. Analysis of the role of transcription factor
1040 VAD-5 in conidiation of *Neurospora crassa*. *Fungal Genet Biol*. 49(5):379-87.

1041

1042 Tanaka S, Brefort T, Neidig N, Djamei A, Kahnt J, Vermerris W, Koenig S, Feussner K, Feussner I, and
1043 Kahmann R. 2014. A secreted *Ustilago maydis* effector promotes virulence by targeting anthocyanin
1044 biosynthesis in maize. *Elife*. 3:e01355.

1045

1046 Telenko DEP, Ross TJ, Shim S, Wang Q, and Singh R. 2020. Draft genome sequence resource for *Phyllachora*
1047 *maydis* - An obligate pathogen that causes tar spot of corn with recent economic impacts in the United States.
1048 *Mol Plant Microbe Interact*. 33(7):884-887.

1049

1050 Teufel F, Armenteros JJA, Johansen AR, Gíslason MH, Pihl SI, Tsirigos KD, Winther O, Brunak S, von Heijne
1051 G, and Nielsen H. 2022. SignalP 6.0 predicts all five types of signal peptides using protein language models.
1052 *Nat Biotechnol*. doi: 10.1038/s41587-021-01156-3.

1053

1054 Thumuluri V, Armenteros JJA, Johansen AR, Nielsen H, Winther O. 2022. DeepLoc 2.0: multi-label subcellular
1055 localization prediction using protein language models. *Nucleic Acids Research* 50( W1):W228–W234.

1056

1057 Törönen P and Holm L. 2021. PANNZER-A practical tool for protein function prediction. *Protein Sci*. 31(1):118-
1058 128.

1059

1060 Tudzynski B. 2014. Nitrogen regulation of fungal secondary metabolism in fungi. *Front Microbiol*. 5: 656.

1061

1062 Vaillancourt B, Buell CR. 2019. High molecular weight DNA isolation method from diverse plant species for
1063 use with Oxford Nanopore sequencing. *BioRxiv.* doi: 10.1101/783159

1064

1065 Valle-Torres J, Ross TJ, Plewa D, Avellaneda MC, Check J, Chilvers MI, Cruz AP, et al. 2020. Tar spot: An
1066 understudied disease threatening corn production in the Americas. *Plant Disease*. 104, 2541– 2550.

1067

1068 Vasara T, Keränen S, Penttilä M, and Saloheimo M. 2002. Characterisation of two 14-3-3 genes from
1069 *Trichoderma reesei*: interactions with yeast secretory pathway components. *Biochim Biophys Acta*. 1590(1-
1070 3):27-40.
1071
1072 Virag A and Harris SD. 2006. Functional characterization of *Aspergillus nidulans* homologues of
1073 *Saccharomyces cerevisiae* Spa2 and Bud6. *Eukaryot Cell*. 5(6): 881–895.
1074
1075 Vurture GW, Sedlazeck FJ, Nattestad M, Underwood CJ, Han Fang H, Gurtowski J, and Schatz MC. 2017.
1076 GenomeScope: fast reference-free genome profiling from short reads. *Bioinformatics*. 33(14): 2202–2204.
1077
1078 Walter P, Gilmore R, Müller M, and Blobel G. 1982. The protein translocation machinery of the endoplasmic
1079 reticulum. *Philos Trans R Soc Lond Ser B Biol Sci*. 300, 225–228.
1080
1081 Walter P, Gilmore R, and Blobel G. 1984. Protein translocation across the endoplasmic reticulum. *Cell*. 38,
1082 5–8.
1083
1084 Wang Q, Pokhrel A and Coleman JJ. 2021. The extracellular superoxide dismutase Sod5 from *Fusarium*
1085 *oxysporum* is localized in response to external stimuli and contributes to fungal pathogenicity. *Front Plant Sci*.
1086 12:608861.
1087
1088 Wang Y, Wu J, Yan J, Guo M, Xu L, Hou L, and Zou Q. 2022. Comparative genome analysis of plant
1089 ascomycete fungal pathogens with different lifestyles reveals distinctive virulence strategies. *BMC Genomics*.
1090 23:34.
1091
1092 Wickham H., et al. (2019). Welcome to the Tidyverse. *J Open Source Softw*. 4(43), 1686.
1093
1094 Wilson AM, Lelwala RV, Taylor PWJ, Wingfield MJ, and Wingfield BD. 2021. Unique patterns of mating
1095 pheromone presence and absence could result in the ambiguous sexual behaviors of *Colletotrichum* species.
1096 *G3 (Bethesda)*. 11(9): jkab187.
1097
1098 Wu J, Wang Y, Park S-Y, Kim SG, Yoo JS, Park S, Gupta R, Kang KY, and Kim ST. 2016. Secreted alpha-N-
1099 arabinofuranosidase B protein is required for the full virulence of *Magnaporthe oryzae* and triggers host
1100 defences. *PLoS One*. 11(10): e0165149.
1101
1102 Xie C, Shang Q, Mo C, Xiao Y, Wang G, Xie J, Jiang D, and Xiao X. 2021. Early secretory pathway-associated
1103 proteins SsEmp24 and SsErv25 are involved in morphogenesis and pathogenicity in a filamentous
1104 phytopathogenic fungus. *mBio*. 12(6): e03173-21.
1105

1106 Xue C, Park G, Choi W, Zheng Li, Dean RA, and Xu J-R. 2002. Two novel fungal virulence genes specifically
1107 expressed in appressoria of the rice blast fungus. *Plant Cell*. 14(9): 2107–2119.
1108
1109 Ying S-H, Liu J, Chu S-L, Xie X-Q, and Feng M-G. 2016. The autophagy-related genes BbATG1 and BbATG8
1110 have different functions in differentiation, stress resistance and virulence of mycopathogen Beauveria
1111 bassiana. *Sci Rep*. 6:26376.
1112
1113 Yu Z and Fischer R. 2019. Light sensing and responses in fungi. *Nat Rev Microbiol*. 17(1):25-36.
1114
1115 Zhao Y, Lim J, Xu J, Yu J-H, and Zheng W. 2020. Nitric oxide as a developmental and metabolic signal in
1116 filamentous fungi. *Mol Microbiol*. 113(5):872-882.
1117
1118 Zhao Z, Liu H, Wang C, and Xu J-R. 2013. Comparative analysis of fungal genomes reveals different plant cell
1119 wall degrading capacity in fungi. *BMC Genomics*. 14:274.
1120

1121

1122 **Figure and Table Legends**

1123

1124 **Figure 1: Genome assembly statistics and mating-type determination**

1125 **(A)** Aerial view of infected tar spot field (top left). Close up of infected leaf tissue (top right courtesy of Jill
1126 Check). Zoomed in view of individual tar spot lesions (bottom left). Spore exudates appear as viscous globular
1127 liquid or dried cirrhi (bottom right courtesy Austin McCoy). **(B)** Yearly spread of tar spot (courtesy of Joe
1128 LaForest https://corn.ipmpipe.org/tarspot/). **(C)** P. maydis genome assembly statistics. **(D)** Illustration of
1129 mating-type locus. **(E)** Genomic Illumina reads mapped to Mat genes and adjacent APN2 and SLA2 genes.
1130 **(F)** Illustration of both pheromone precursor loci. **(G)** Illustration of both pheromone receptor loci.

1131

1132 **Figure 2: Comparative genomics between *P. maydis* and sordariomycetes**

1133 **(A)** Conservation or absence of KEGG K-numbers between *P. maydis* and all sordariomycetes within the
1134 KEGG database. **(B)** Presence (blue) and absence (red) of known inorganic nitrogen utilization genes *in P.*
1135 *maydis* in comparison to all sordariomycetes within the KEGG database.

1136

1137 **Figure 3: Cellular and metabolic pathway expression**

1138 **(A)** Average metabolic pathway TPM values. **(B)** Average cellular process pathway TPM values. Circle size
1139 corresponds to number of genes within the pathway. Circle color corresponds to average pathway expression
1140 from low (blue) to high (red).

1141

1142 **Figure 4: Transporter, light-sensing, and reproductive gene expression**

1143 **(A)** Mean TPM of identified transporters. **(B)** Illustration of identified light-sensing proteins and downstream
1144 regulated proteins. **(C)** Mean TPM of well-studied genes involved in light sensing, nutrient sensing, mate
1145 recognition, reproduction regulation, and sexual and asexual reproduction.

1146

1147 **Figure 5: Expression analysis of secreted enzymes and effectors**

1148 **(A)** Identification of conserved and unique secreted enzymes encoded by *P. maydis* using an $e^{-20}$ threshold
1149 (left). Quantity of glycoside hydrolases (GH), auxiliary activities (AA), carbohydrate esterases (CE),
1150 carbohydrate-binding (CB), and glycosyltransferases (GT) CAZymes (middle). Mean expression of CAZymes
1151 (right). **(B)** Identification of conserved and unique secreted effectors encoded by *P. maydis* using an $e^{-20}$
1152 threshold (left). Predicted host localization of conserved and unique effectors (middle). Mean expression of
1153 effectors (right).

1154

1155 **Supplemental Figure 1: Genome features**

1156 **(A)** K-mer-based genome size prediction. **(B)** Repetitive DNA quantification and characterization. **(C)** Predicted
1157 localization of proteins encoded by *P. maydis*.

1158

1159 **Supplemental Figure 2: Expanded expression of genes in pathways**

1160 **(A)** Expanded metabolic pathway average expression including oxidative phosphorylation. **(B)** Schematic of
1161 ammonia and glutamine utilization genes in fungi (top). Average TPM values for genes involved in this process
1162 (bottom). **(C)** Mean TPM for each gene within the DNA replication KEGG pathway. **(D)** Mean TPM for each
1163 gene within the meiosis KEGG pathway. **(E)** Mean TPM for each gene within the autophagy KEGG pathway.
1164 Genes are colored red or blue depending on whether they have been previously implicated for their
1165 involvement in pathogenicity or pathogenicity and conidiation, respectively **(F)** Microscopy images of perithecia
1166 containing asci. **(G)** Microscopy images of pycnidia containing conidia.

1167

1168 **Supplemental Table 1**

1169 KEGG orthology groups absent in PM02 genome and present in various Sordariomycete species (designated
1170 by their KEGG organism code).

1171

1172 **Supplemental Table 2**

1173 PM02 annotated gene list with expression levels (TPM) and functional annotation.

1174

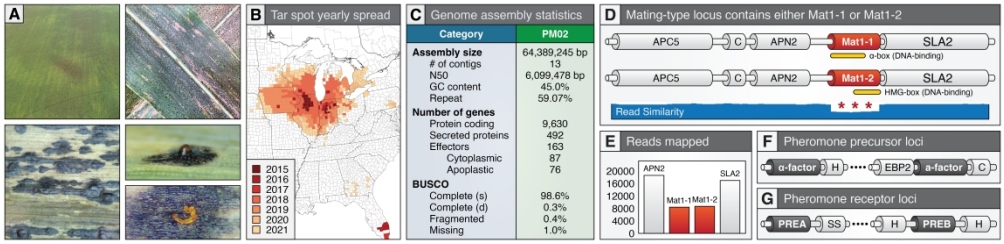


Figure 1: Genome assembly statistics and mating-type determination
(A) Aerial view of infected tar spot field (top left). Close up of infected leaf tissue (top right courtesy of Jill Check). Zoomed in view of individual tar spot lesions (bottom left). Spore exudates appear as viscous globular liquid or dried cirrhi (bottom right courtesy Austin McCoy). (B) Yearly spread of tar spot (courtesy of Joe LaForest https://corn.ipmpipe.org/tarspot/). (C) P. maydis genome assembly statistics. (D) Illustration of mating-type locus. (E) Genomic Illumina reads mapped to Mat genes and adjacent APN2 and SLA2 genes. (F) Illustration of both pheromone precursor loci. (G) Illustration of both pheromone receptor loci.

441x107mm (394 x 394 DPI)

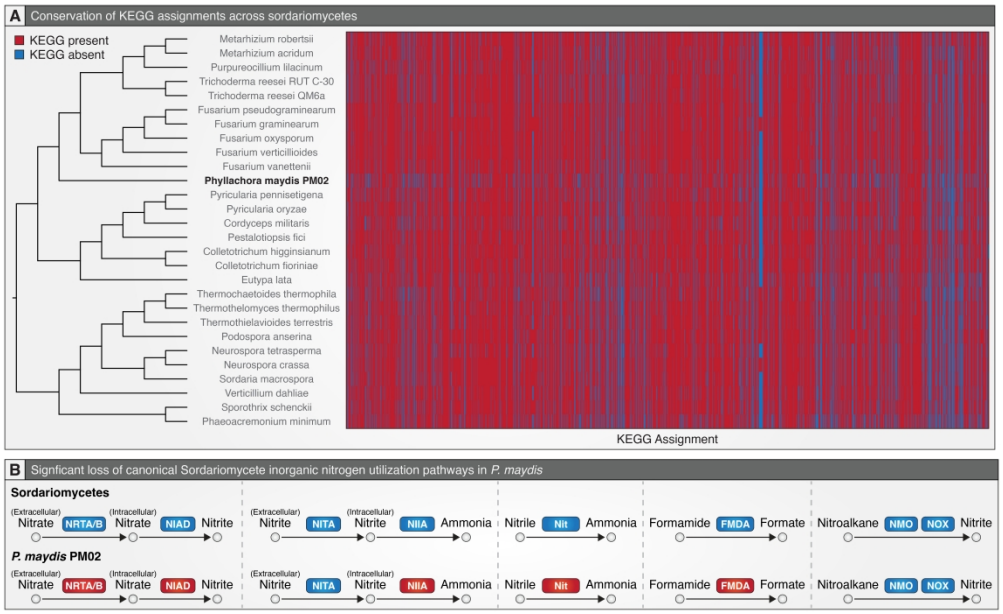


Figure 2: Comparative genomics between P. maydis and sordariomycetes
(A) Conservation or absence of KEGG K-numbers between P. maydis and all sordariomycetes within the KEGG database. (B) Presence (blue) and absence (red) of known inorganic nitrogen utilization genes in P. maydis in comparison to all sordariomycetes within the KEGG database.

441x270mm (394 x 394 DPI)

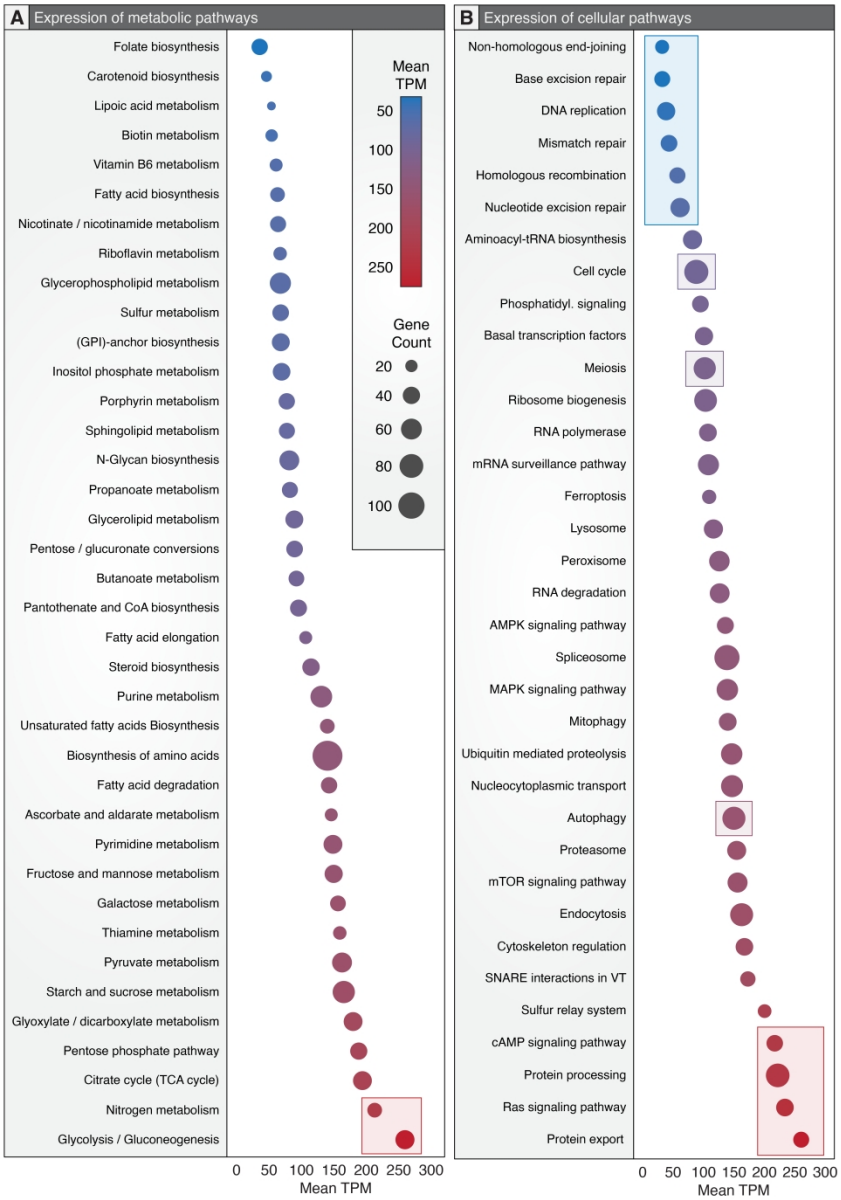


Figure 3: Cellular and metabolic pathway expression
(A) Average metabolic pathway TPM values. (B) Average cellular process pathway TPM values. Circle size corresponds to number of genes within the pathway. Circle color corresponds to average pathway expression from low (blue) to high (red).

306x434mm (394 x 394 DPI)

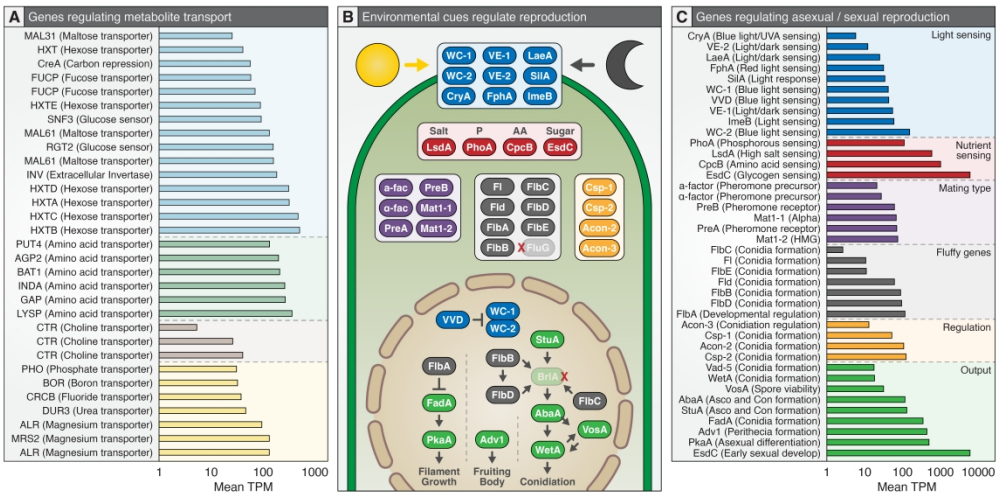


Figure 4: Transporter, light-sensing, and reproductive gene expression
(A) Mean TPM of identified transporters. (B) Illustration of identified light-sensing proteins and downstream regulated proteins. (C) Mean TPM of well-studied genes involved in light sensing, nutrient sensing, mate recognition, reproduction regulation, and sexual and asexual reproduction.

441x218mm (394 x 394 DPI)

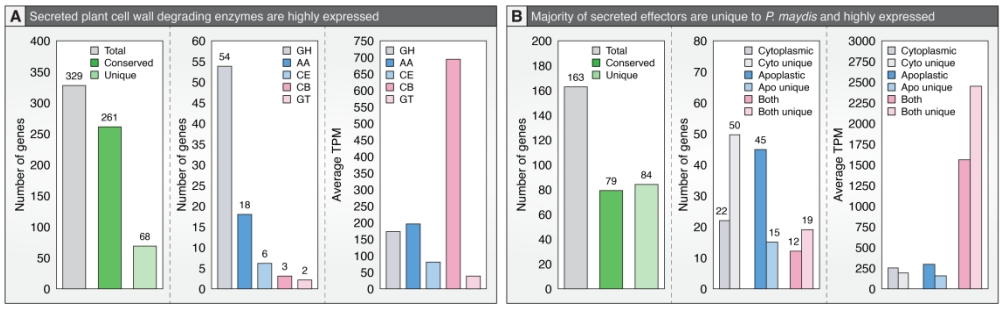


Figure 5: Expression analysis of secreted enzymes and effectors
(A) Identification of conserved and unique secreted enzymes encoded by P. maydis using an e-20 threshold (left). Quantity of glycoside hydrolases (GH), auxiliary activities (AA), carbohydrate esterases (CE), carbohydrate-binding (CB), and glycosyltransferases (GT) CAZymes (middle). Mean expression of CAZymes (right). (B) Identification of conserved and unique secreted effectors encoded by P. maydis using an e-20 threshold (left). Predicted host localization of conserved and unique effectors (middle). Mean expression of effectors (right).

441x136mm (394 x 394 DPI)

## Supplemental Figures

**A** P. maydis genome size estimation

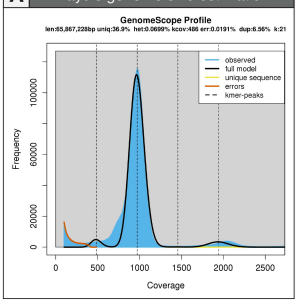


**B** P. maydis genome contains significant repetitive content

| Order | Superfamily | Count | BP | % |
|---|---|---|---|---|
| **Class I (retrotransposons)** | | 35,310 | 34,916,388 | 54.28% |
| LTR | Copia | 23,596 | 20,639,486 | 32.09% |
| | Gypsy | 143 | 633,120 | 0.98% |
| | Unknown | 11,571 | 13,643,782 | 21.21% |
| **Class II (DNA transposons)** | | 2,658 | 18,93,398 | 2.95% |
| TIR | CACTA | 15 | 35,550 | 0.06% |
| | Mutator | 893 | 193,036 | 0.30% |
| | PIF_Harbinger | 24 | 41,245 | 0.06% |
| | Tc1_Mariner | 1,724 | 16,18,563 | 2.52% |
| | hAT | 2 | 5,004 | 0.01% |
| **Non-TIR** | Helitron | 3 | 20,047 | 0.03% |
| **Repeat_Region** | | 3,378 | 11,62,664 | 1.81% |
| **Total** | | 41,349 | 37,992,497 | 59.07% |

**C** DeepLoc 2.0 subcellular localization prediction

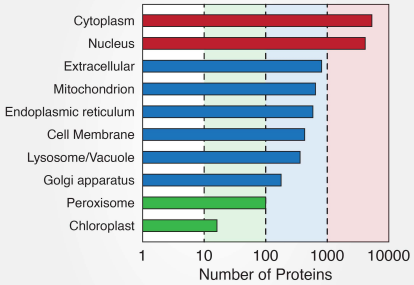


**Supplemental Figure 1: Genome features**
**(A)** Kmer-based genome size prediction. **(B)** Repetitive DNA quantification and characterization. **(C)** Predicted localization of proteins encoded by *P. maydis*.

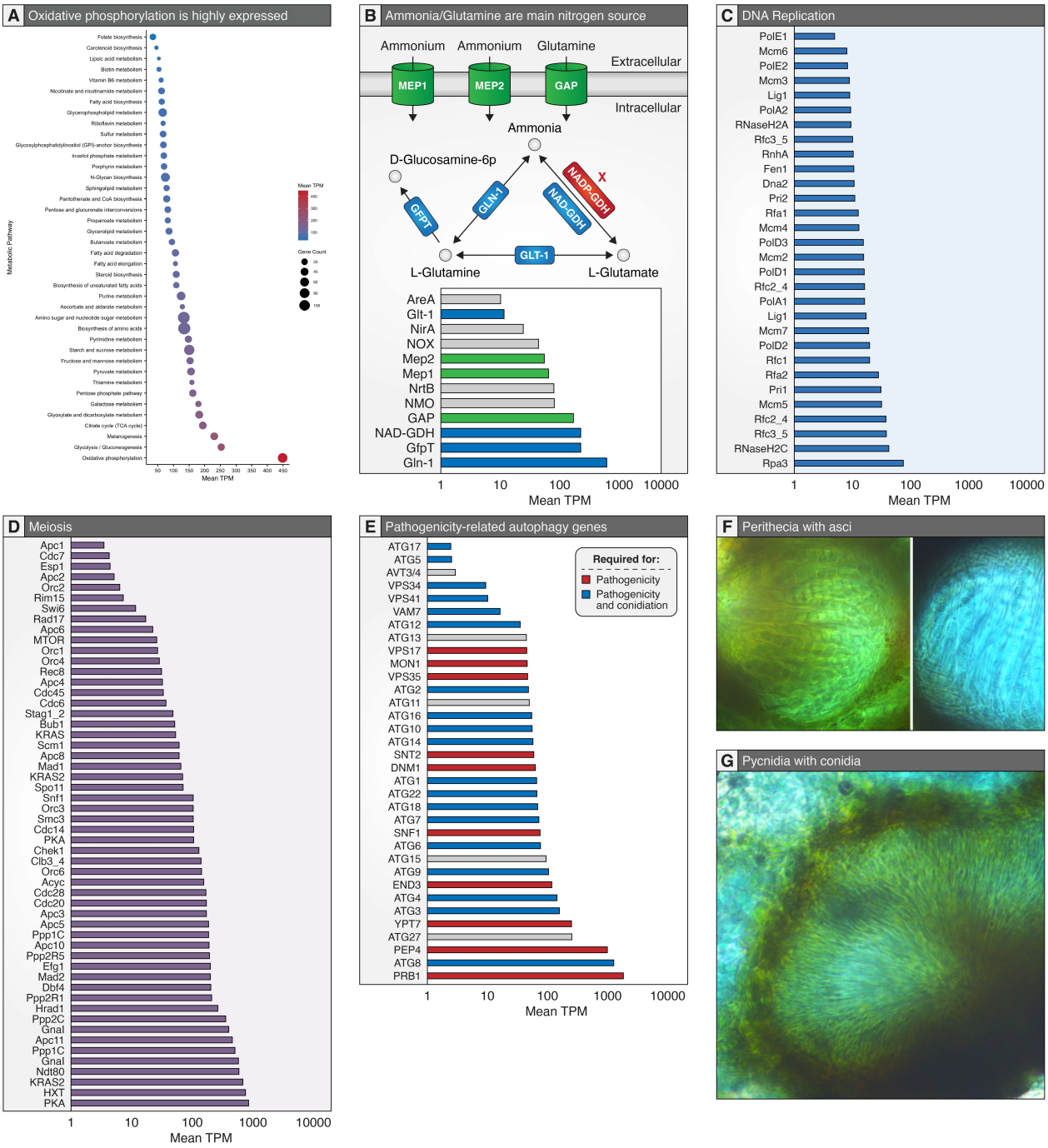


**Supplemental Figure 2: Expanded expression of genes in pathways**

**(A)** Expanded metabolic pathway average expression including oxidative phosphorylation. **(B)** Schematic of ammonia and glutamine utilization genes in fungi (top). Average TPM values for genes involved in this process (bottom). **(C)** Mean TPM for each gene within the DNA replication KEGG pathway. **(D)** Mean TPM for each gene within the meiosis KEGG pathway. **(E)** Mean TPM for each gene within the autophagy KEGG pathway. Genes are colored red or blue depending on whether they have been previously implicated for their involvement in pathogenicity or pathogenicity and conidiation, respectively **(F)** Microscopy images of perithecia containing asci. **(G)** Microscopy images of pycnidia containing conidia.